Workshop on Qualitative and Quantitative Approaches to Inverse Scattering Problems
Institute for Mathematical Sciences, National University of Singapore
September 27, 2018

Microwave Near-field Imaging in Real Time

Natalia K. Nikolova
nikolova@ieee.org

McMaster University
Department of Electrical and Computer Engineering
Electromagnetic Vision (EMVi) Research Laboratory
Hamilton, ON CANADA

APPLICATIONS OF MICROWAVE NEAR-FIELD IMAGING

- penetration into optically obscured objects (clothing, walls, luggage, living tissue…)
  - ➢ the lower the frequency the better the penetration
  - ➢ frequency bands from 500 MHz into the mm-wave bands (≤300 GHz)
- compact relatively cheap electronics esp. in the low-GHz range
- diverse suite of image reconstruction methods

VARIOUS APPLICATIONS

whole body scanners

nondestructive testing

through-wall imaging

medical imaging

underground radar

APPLICATIONS: LUGGAGE INSPECTION, NDT

[Ghasr *et al.*, "Wideband microwave camera for real-time 3-D imaging," *IEEE Trans. AP*, 2017]

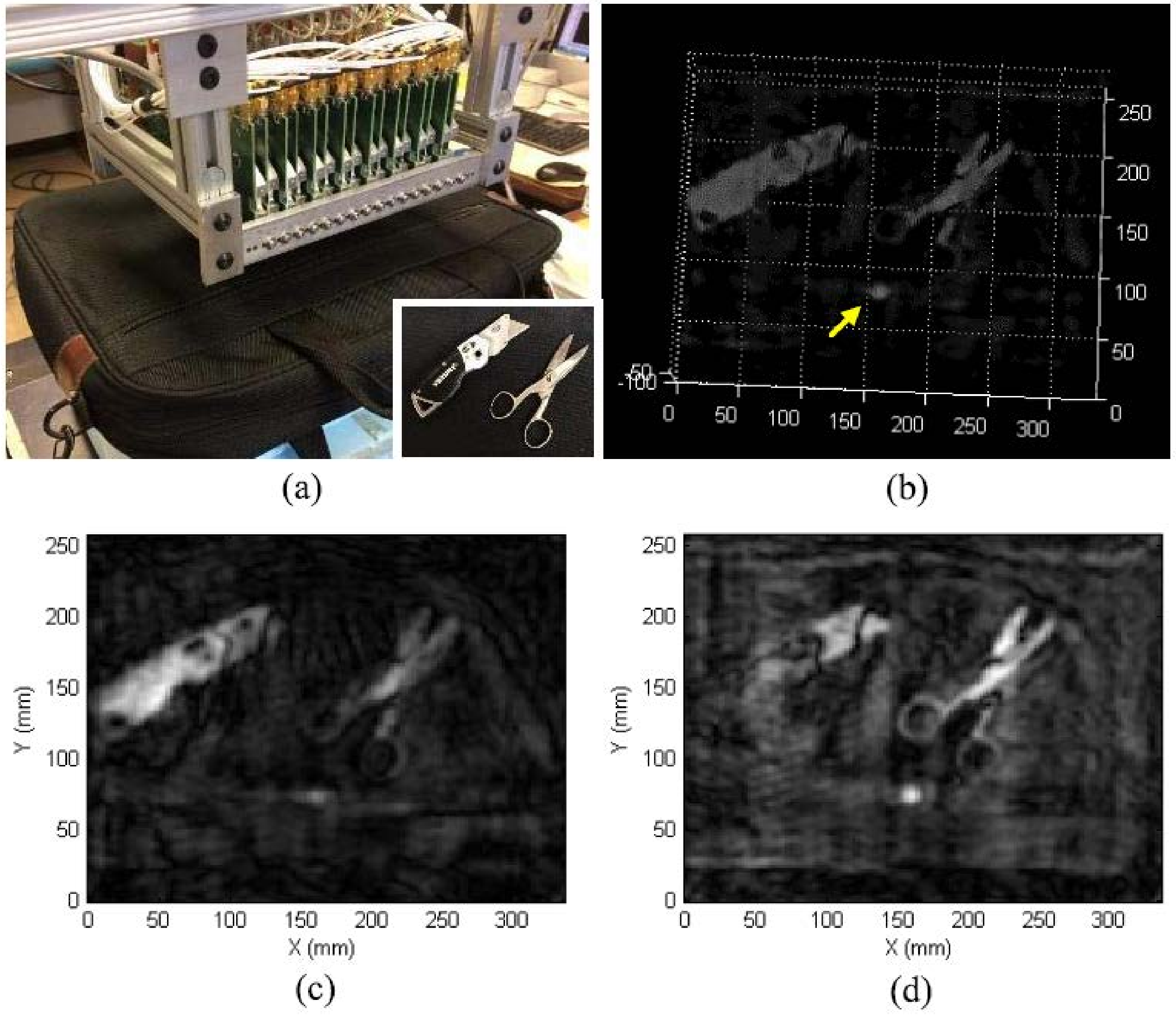

20 GHz to 30 GHz frequency range

Prof. Zoughi's team at Missouri University of Science & Technology

video

[https://youtu.be/RE-PPXmtTeA]

Fig. 15. Example of video camera utility for imaging a box cutter and a pair of scissors inside a laptop bag. (a) Picture of laptop bag in front of the camera aperture with inset showing the objects inside the bag. (b) 3-D view. (c) 2-D image slice focused on the box cutter. (d) 2-D image slice focused on the pair of scissors.

APPLICATIONS: WHOLE BODY SCANNERS

[Sheen *et al.*, “Near-field three-dimensional radar imaging techniques and applications,” *Applied Optics* 2010]

Pacific Northwest National Laboratory, Washington, USA

40 GHz to 60 GHz (U band) cylindrical scan

40 GHz to 60 GHz (U band) cylindrical scan

10 GHz to 20 GHz polarimetric cylindrical scan

APPLICATIONS: MEDICAL IMAGING

[Song *et al.*, "Detectability of breast tumor by a hand-held impulse-radar detector: performance evaluation and pilot clinical study," *Nature Sci. Reports* 2017]

Prof. Kikkawa's team at Hiroshima University, Japan

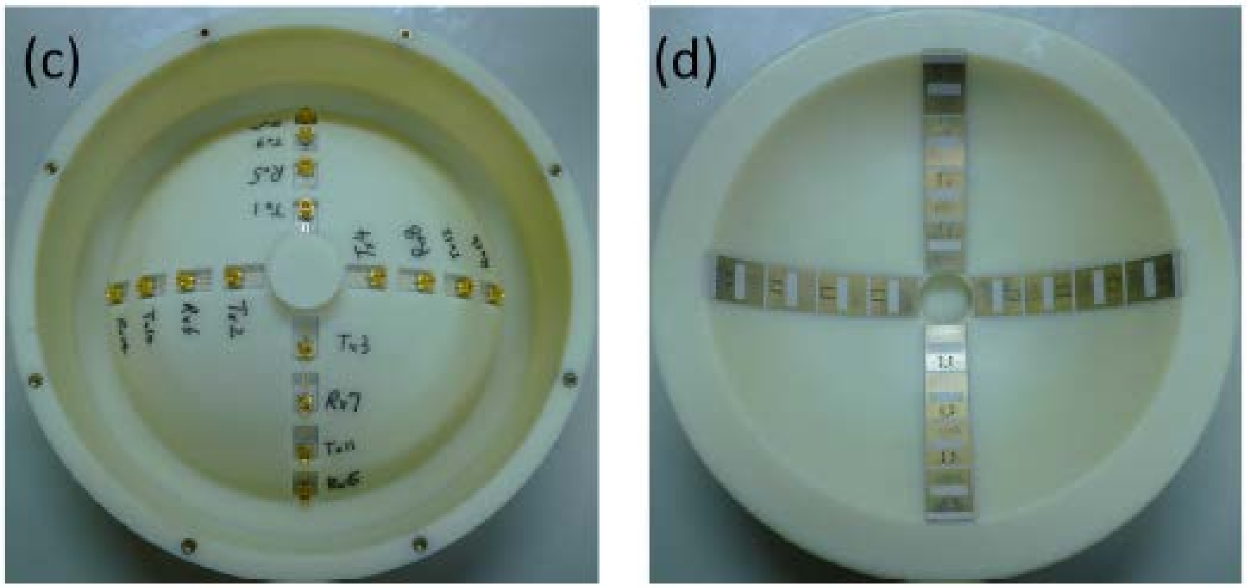

Figure 3. Dome antenna array design. (**a**) The top view of the antenna in x-y plane. (**b**) The side view of the antenna in x-z plane. (**c**) Top view photograph. (**d**) Bottom view photograph.

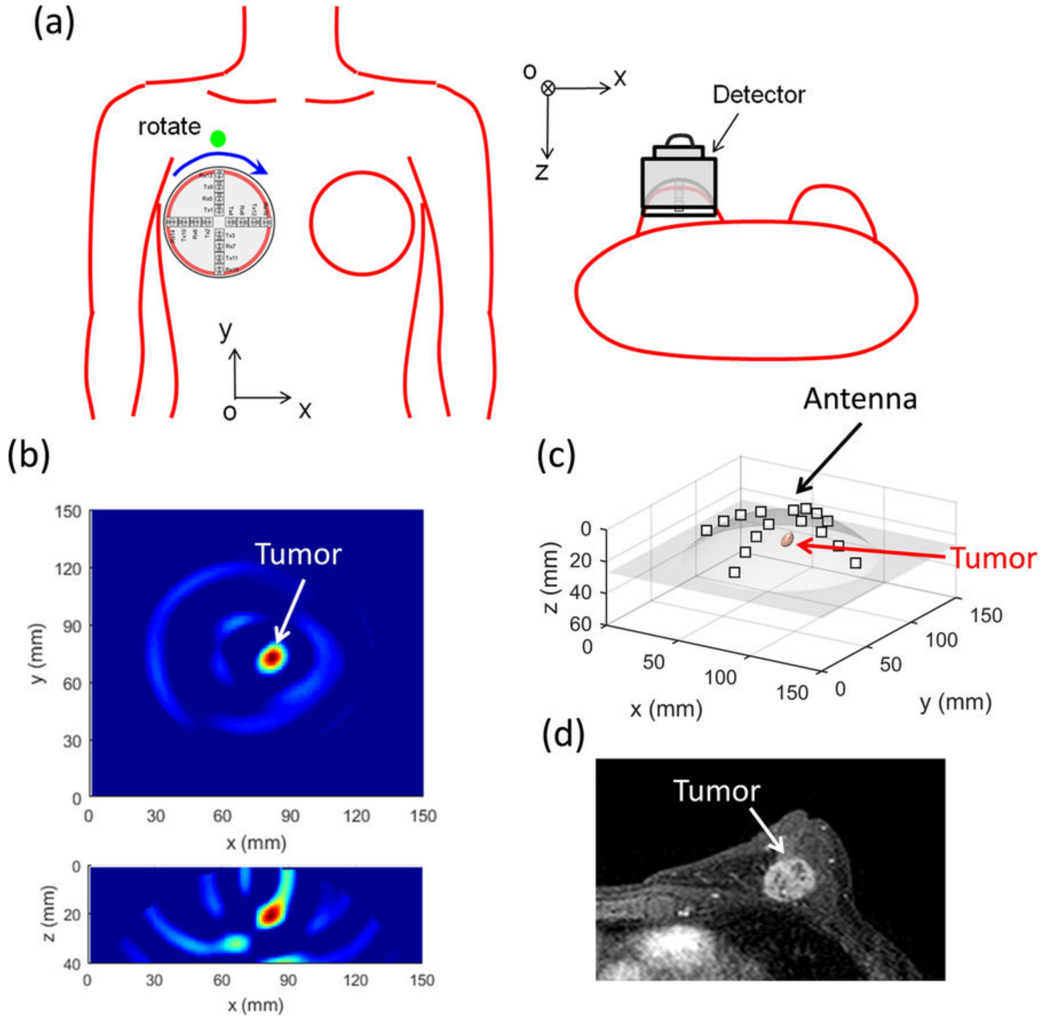

MICROWAVE NEAR-FIELD IMAGING: COMMERCIAL GROWTH

- mm-wave whole-body imagers for airport security inspection (> 30 GHz)
- through-wall and through-floor infrastructure inspection for contractors and home inspectors (UWB, 3 GHz to 8 GHz)
- numerous underground radar applications: detection of pipes, cables, tunnels, etc. (< 3 GHz)

[video credit: https://www.youtube.com/watch?v=_YZEa1hiGO0]

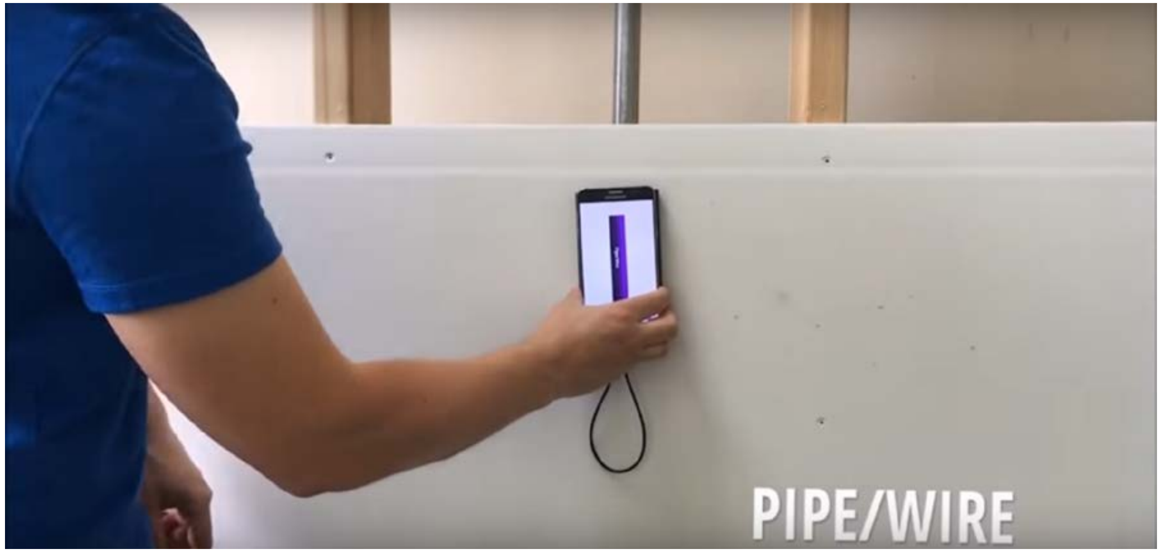

[video credit: https://walabot.com/diy]

OUTLINE

- **specifics of near-field microwave imaging in**
  - data acquisition
  - forward models
  - inversion strategies (real-time)

- **examples and comparisons of methods**

DATA ACQUISITION: SCANNING

Principle: *N*-D imaging (*N*=2,3) needs *abundant* and *diverse* *N*-D data sets

- **spatial scans** – 1D (linear) or 2D (surface)
  - illuminate target from various angles
  - collect scattered signals at various angles/distances
  - acquisition surfaces – planar, cylindrical, spherical
  - mechanical vs. electronic scanning

	mechanical scan	electronic switching
speed	low	HIGH
complexity	LOW	high
flexibility in adjusting scan parameters	GREAT	limited

- **frequency/temporal sweeps**
- **polarization diversity**

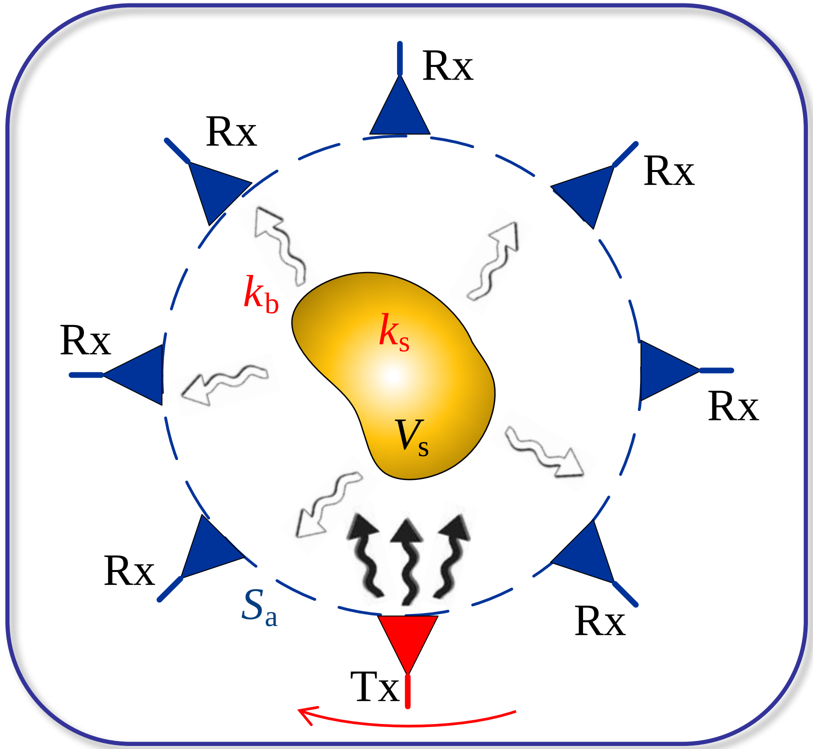

DATA ACQUISITION: SPATIAL SAMPLING

- spatial data diversity
  - each sample must add independent information – improves uniqueness
  - linearly dependent data may lead to ill-posed inversion problems
  - over-sampling: pros and cons
  - staying below but close to the ***maximum spatial sampling step*** ensures diversity

$$\boxed{\Delta\zeta \le \Delta\zeta_{\max} \approx \frac{\lambda_{\min}}{4\sin\alpha},\ \zeta \equiv x, y}$$

  - ***effective near-field wavelengths*** may be shorter than $\lambda = 2\pi / k_{\mathrm{b}}$

$$\boxed{\lambda_{\mathrm{eff,min}} = \frac{2\pi}{k_{x,y}^{\max}}}$$

$$\tilde{S}(k_x, k_y) = \mathcal{F}_{2\mathrm{D}}\{S(x, y)\}$$

$$\boxed{\alpha = \min(\alpha_{\mathrm{A,max}}, \Omega_{\mathrm{A}} / 2)}$$

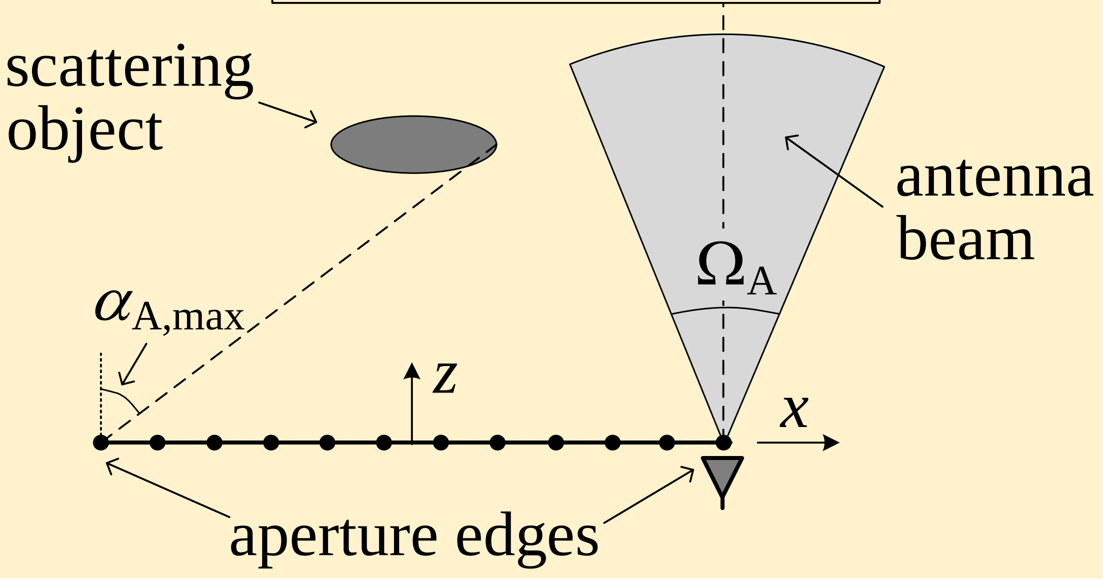

DATA ACQUISITION: FREQUENCY SAMPLING

- frequency data diversity in frequency-sweep measurements
  - stay below but close to the ***maximum frequency sampling step***
  - ensures that back-scattered signals (after IFFT) from all targets at distances $\leq R_{\max}$ do not overlap

$$\boxed{\Delta f \leq \Delta f_{\max} = \frac{1}{2T_{\max}} \approx \frac{v_{\mathrm{b}}}{4R_{\max}}}$$

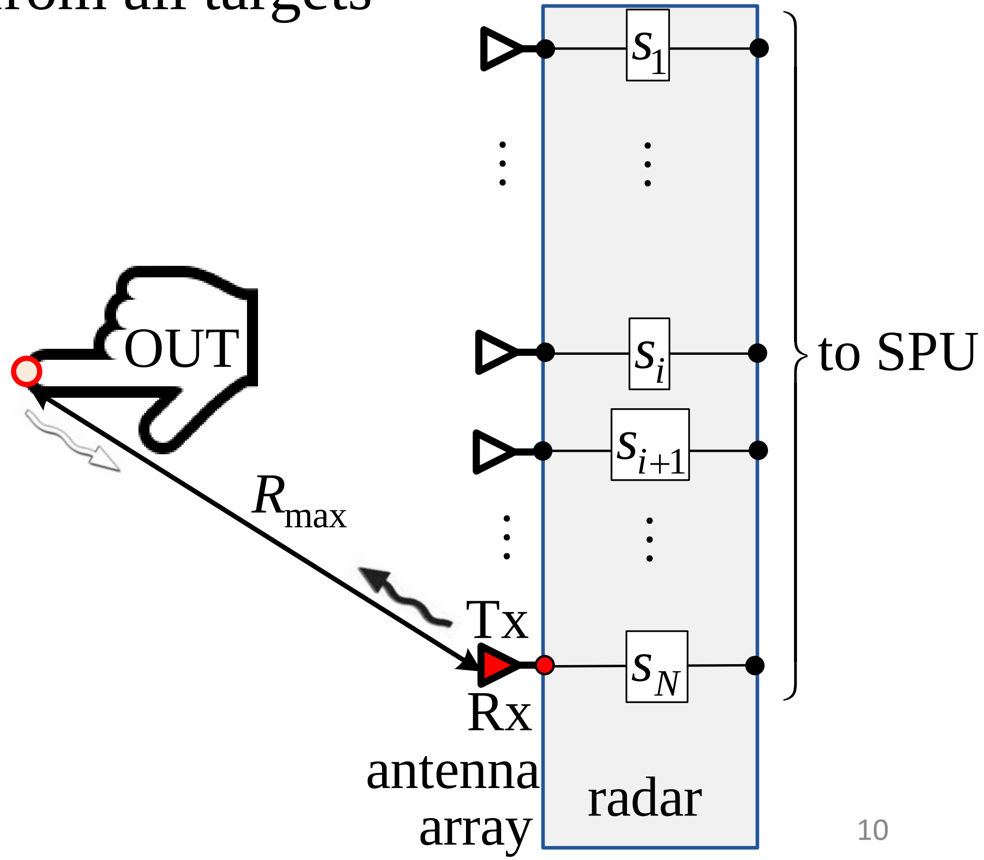

DATA ACQUISITION: TEMPORAL SAMPLING

- temporal data diversity in time-domain measurements
  - stay below but close to the ***maximum time sampling step***
  - ensures that all frequency components of the pulsed signals are fully used (Nyquist)

$$\boxed{\Delta t \le \Delta t_{\mathrm{max}} \approx \frac{T_{\mathrm{min}}}{2} = \frac{1}{2 f_{\mathrm{max}}}}$$

FORWARD MODEL OF SCATTERING: *S*-PARAMETER DATA EQUATION

[Nikolova *et al.*, *APS-URSI* 2016][Beaverstone *et al.*, *IEEE Trans. MTT*, 2017]

- scattering from penetrable objects (isotropic scatterer)

$$\underbrace{S_{ik}^{\mathrm{sc}}}_{\text{data}} = \underbrace{\frac{\mathrm{i}\omega\varepsilon_0}{2a_i a_k}}_{\text{known constants}} \iiint_{V_s} \Delta\varepsilon_r(\mathbf{r}')\,\mathbf{E}_i^{\mathrm{inc}}(\mathbf{r}')\cdot\mathbf{E}_k^{\mathrm{tot}}(\mathbf{r}')\,d\mathbf{r}'$$

$$\Delta\varepsilon_r(\mathbf{r}') = \varepsilon_r(\mathbf{r}') - \varepsilon_{r,\mathrm{b}}(\mathbf{r}')$$

data

complex permittivity contrast

Green's vector function

total internal field

$\mathbf{E}_i^{\mathrm{inc}}(\mathbf{r}')$: incident internal field due to Rx antenna if it were to transmit

$\mathbf{E}_k^{\mathrm{tot}}(\mathbf{r}')$: total internal field due to Tx antenna

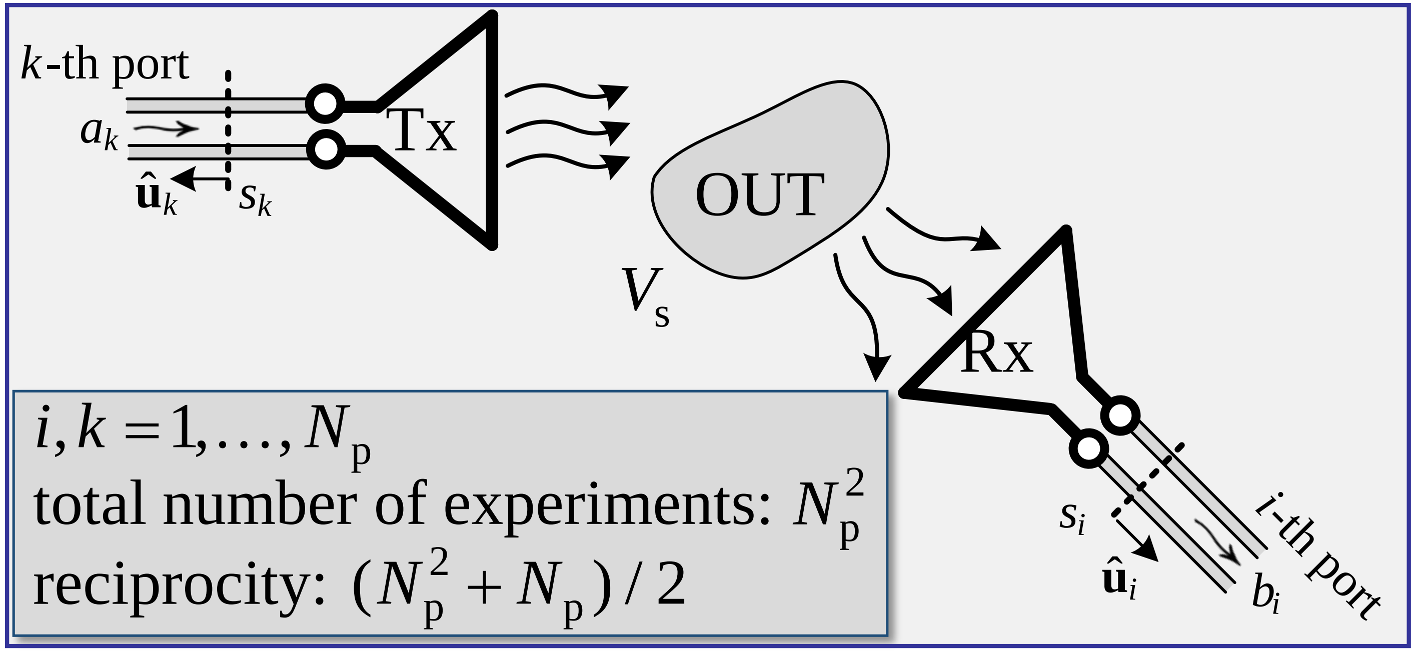

FORWARD MODEL: BORN'S LINEARIZING APPROXIMATION

$$\boxed{S_{ik}^{\mathrm{sc}} = \frac{\mathrm{i}\omega\varepsilon_0}{2a_i a_k} \iiint_{V_s} \Delta\varepsilon_r(\mathbf{r}')\mathbf{E}_i^{\mathrm{inc}}(\mathbf{r}') \cdot \mathbf{E}_k^{\mathrm{tot}}\left(\mathbf{r}'; \Delta\varepsilon_r(\mathbf{r}')\right) d\mathbf{r}'}$$

data

contrast (to be found)

Green's function

total internal field

- total field $\mathbf{E}_k^{\mathrm{tot}}\left(\mathbf{r}'; \Delta\varepsilon(\mathbf{r}')\right)$ is generally unknown and depends on contrast: ***data equation is nonlinear in the unknown contrast***
- Born's approximation of the total internal field linearizes the data equation:

$$\boxed{\mathbf{E}_k^{\mathrm{tot}}\left(\mathbf{r}'; \Delta\varepsilon(\mathbf{r}')\right) \approx \mathbf{E}_k^{\mathrm{inc}}(\mathbf{r}')} \qquad \Rightarrow S_{ik}^{\mathrm{sc}} \approx \iiint_{V_s} \Delta\varepsilon_r(\mathbf{r}') \underbrace{\bar{\mathbf{E}}_i^{\mathrm{inc}}(\mathbf{r}') \cdot \bar{\mathbf{E}}_k^{\mathrm{inc}}(\mathbf{r}')}_{\substack{\text{resolvent kernel} \\ \text{(assumed known)}}} d\mathbf{r}'$$

- main challenge of near-field imaging with linear inversion methods:

  incident-field distributions in antennas' near zone are difficult to model

FORWARD MODEL: FAR-ZONE vs. NEAR-ZONE ANTENNA FIELDS

any one of the conditions below implies near-field (short-range) imaging

- object is in the near-field region of antennas $r < D_{\text{far}} \approx \dfrac{2D_{\text{A,max}}^2}{\lambda}$
- distance from object to antennas ≤ object's size $r \le D_{\text{OUT,max}}$
- distance from object to antennas ≤ wavelength $r \le \lambda$

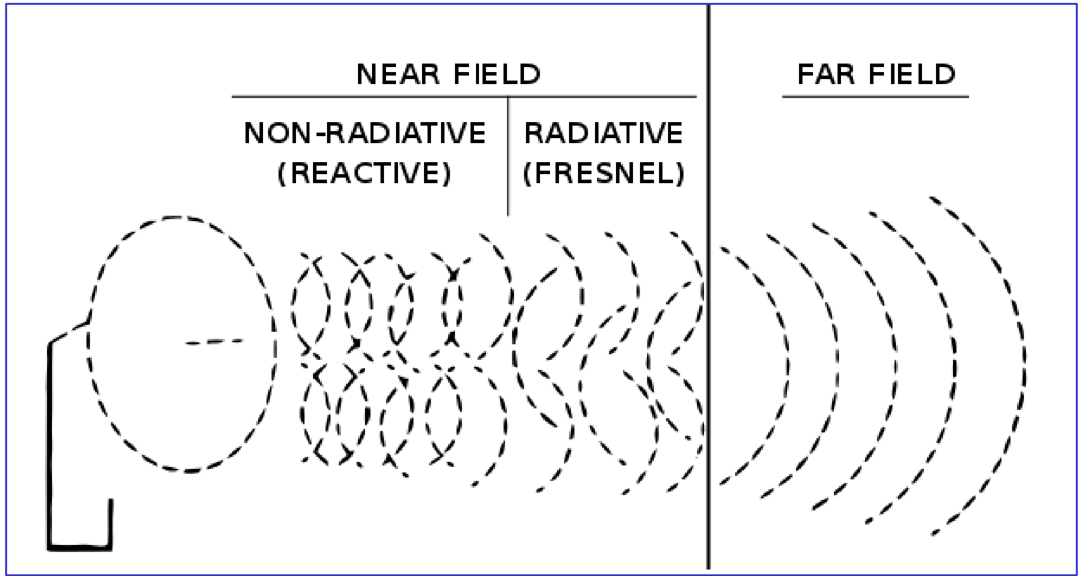

Goran M Djuknic - US Patent 6657596,
commons.wikimedia.org/w/index.php?curid=20417988

- implication: ***resolvent kernel depends on incident fields which do not conform to analytical free-space far-zone propagation models***, e.g.,

$$\mathbf{E}^{\text{inc}}(\mathbf{r}') \sim \hat{\mathbf{p}} G(\theta,\varphi) \frac{e^{-\text{i}k_{\text{b}}r}}{r} \longleftarrow \textit{not valid}$$

LINEARIZED FORWARD MODEL: TIME DOMAIN

- Born's linearizing approximation is applied in the same way

frequency-domain (S-parameters)

$$S_{ik}^{\mathrm{sc}} \approx \iiint_{V_s} \Delta\varepsilon_r(\mathbf{r}')\overline{\mathbf{E}}_i^{\mathrm{inc}}(\mathbf{r}')\cdot\overline{\mathbf{E}}_k^{\mathrm{inc}}(\mathbf{r}')d\mathbf{r}'$$

time-domain (pulsed-radar waveforms)

$$\boxed{s^{\mathrm{sc}}(\mathbf{r}_{\mathrm{Rx}},t;\mathbf{r}_{\mathrm{Tx}}) \approx \iiint_{V_s} \kappa(\mathbf{r}')\left[h_{\mathrm{Rx}}^{\mathrm{inc}} * (u_{\mathrm{Tx}}^{\mathrm{inc}})''\right]_{(\mathbf{r}_{\mathrm{Rx}},t;\mathbf{r}_{\mathrm{Tx}};\mathbf{r}')} d\mathbf{r}'} \qquad \kappa(\mathbf{r}') = \frac{\Delta\varepsilon_r}{v_{\mathrm{b}}^2}$$

data (known)

contrast (unknown)

impulse response of Rx incident field (assumed known)

Tx incident field (assumed known)

[Nikolova, *Introduction to Microwave Imaging*, 2017]

LINEARIZED FORWARD MODEL: BORN vs. RYTOV DATA APPROXIMATION

- Born scattered-field data approximation

$$S_{ik}^{\mathrm{sc}}(\mathbf{r} \in S_{\mathrm{a}}) \approx \underbrace{\left[S_{ik}^{\mathrm{tot}} - S_{ik}^{\mathrm{inc}}\right]_{(\mathbf{r}\in S_{\mathrm{a}})}}_{\text{data calibration step}} \approx \iiint_{V_{\mathrm{s}}} \Delta\varepsilon_r(\mathbf{r}')\bar{\mathbf{E}}_i^{\mathrm{inc}}(\mathbf{r}') \cdot \bar{\mathbf{E}}_k^{\mathrm{inc}}(\mathbf{r}')d\mathbf{r}'$$

- Rytov scattered-field data approximation

$$S_{ik}^{\mathrm{sc}}(\mathbf{r} \in S_{\mathrm{a}}) \approx \underbrace{S_{ik}^{\mathrm{inc}} \ln\left(\frac{S_{ik}^{\mathrm{tot}}}{S_{ik}^{\mathrm{inc}}}\right)_{\mathbf{r}\in S_{\mathrm{a}}}}_{\text{data calibration step}} \approx \iiint_{V_{\mathrm{s}}} \Delta\varepsilon_r(\mathbf{r}')\bar{\mathbf{E}}_i^{\mathrm{inc}}(\mathbf{r}') \cdot \bar{\mathbf{E}}_k^{\mathrm{inc}}(\mathbf{r}')d\mathbf{r}'$$

[Tajik *et al.*, *JPIER- B*, 2017][Shumakov *et al.*, *Trans. MTT*, 2018]

FORWARD MODEL: APPROXIMATIONS

- **total internal field approximation (Born)**
  - limitations on both size and contrast of the scatterer

$$a^2 \left| k_s^2(\mathbf{r}) - k_b^2 \right| \ll 1,\ \mathbf{r} \in V_s$$

[Nikolova, *Introduction to Microwave Imaging*, 2017]

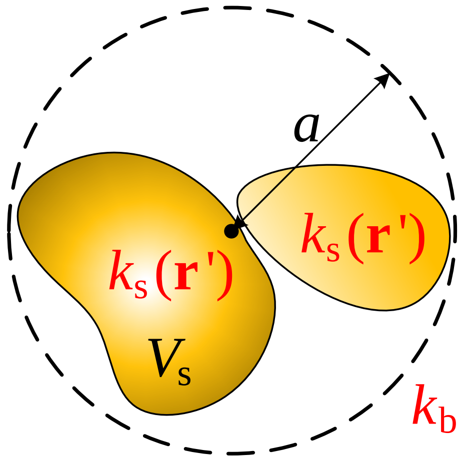

  - if OUT violates limit: image contains artifacts which reflect differences between $\mathbf{E}_{\mathrm{Tx}}^{\mathrm{inc}}(\mathbf{r}')$ and $\mathbf{E}_{\mathrm{Tx}}^{\mathrm{tot}}(\mathbf{r}')$ rather than contrast
  - expect trouble in areas of strong multiple scattering & mutual coupling

- **data approximation**
  - Born – limitation on both size and contrast: $2a\left| k_s(\mathbf{r}) - k_b \right| < \pi,\ \mathbf{r} \in S_a$
  - Born – neglects multiple scattering & mutual coupling between antennas and OUT
  - Rytov – limitation on contrast only: $\left(k_s^2 - k_b^2\right) / k_b^2 < 1,\ \mathbf{r} \in S_a$

LINEAR INVERSION METHODS: THE ENGINES OF REAL-TIME IMAGING

principle: linearize forward model & solve resulting linear system of equations

$$\boxed{S_{ik}^{\mathrm{sc}} \approx \iiint_{V_s} \Delta\varepsilon_r(\mathbf{r}')\underbrace{\overline{\mathbf{E}}_i^{\mathrm{inc}}(\mathbf{r}')\cdot\overline{\mathbf{E}}_k^{\mathrm{inc}}(\mathbf{r}')}\,d\mathbf{r}'}$$

data (known)

contrast (unknown)

normalized incident fields (assumed known)

- contrast and compare with nonlinear inversion methods

principle: solve nonlinear forward-model equations for BOTH contrast and total field using nonlinear optimization and/or iterative methods

$$\boxed{S_{ik}^{\mathrm{sc}} \approx \iiint_{V_s} \Delta\varepsilon_r(\mathbf{r}')\overline{\mathbf{E}}_i^{\mathrm{inc}}(\mathbf{r}')\cdot\overline{\mathbf{E}}_k^{\mathrm{tot}}\left(\mathbf{r}';\Delta\varepsilon_r(\mathbf{r}')\right)d\mathbf{r}'} + \text{Maxwell's equations}$$

data (known)

contrast (unknown)

Green's function (assumed known)

total internal field (unknown)

RECONSTRUCTION WITH FREQUENCY-SWEEP DATA: **HOLOGRAPHY**

holography refers to reconstruction methods that use both the magnitude and phase of the scattered waves recorded at a surface to produce a 3D image in a single inversion step

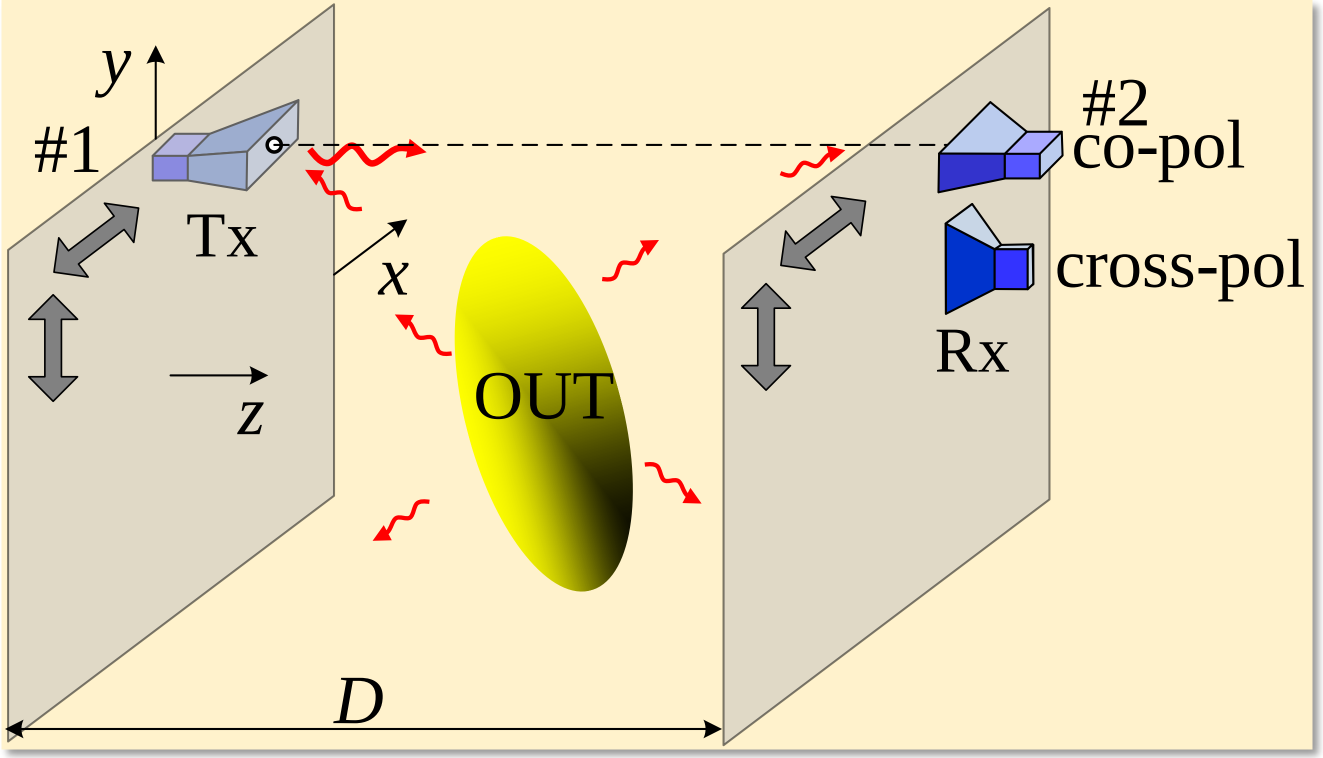

type of response	**number of values** $S_{ik}(x',y')$
co-pol X-X	$4\text{x}N_\omega$
co-pol Y-Y	$4\text{x}N_\omega$
cross-pol X-Y	$4\text{x}N_\omega$
cross-pol Y-X	$4\text{x}N_\omega$
TOTAL	$16\text{x}N_\omega = N_T$

number of responses acquired at each position

- reflected signals: S_{11}, S_{22}
- transmitted signals: S_{21}, S_{12}

for a pair of antennas

HOLOGRAPHY: RESOLVENT KERNEL

$$S_\xi^{\text{sc}}(x,y,\overline{z};\omega) \approx \iiint_{V_s} \Delta\varepsilon_r(x',y',z') \underbrace{\left[\overline{\mathbf{E}}_{\xi,\text{Rx}}^{\text{inc}} \cdot \overline{\mathbf{E}}_{\xi,\text{Tx}}^{\text{inc}}\right]_{(x',y',z';x,y,\overline{z};\omega)}}_{\text{approximate (Born) resolvent kernel } \mathcal{K}_\xi(\mathbf{r}';\mathbf{r};\omega)} dx'dy'dz', \; \xi = 1,\ldots,N_T$$

- assume kernel is translationally invariant in x and y (background is uniform or layered)

Let $\mathcal{K}_{0,\xi}(x',y';z';\omega)$

$$\equiv \mathcal{K}_\xi(x',y',z';\overbrace{0,0,\overline{z}}^{\text{antennas at aperture center}};\omega)$$

Then $\mathcal{K}_\xi(x',y',z';x,y,\overline{z};\omega) =$

$$\mathcal{K}_{0,\xi}(x'-x,y'-y;z';\omega)$$

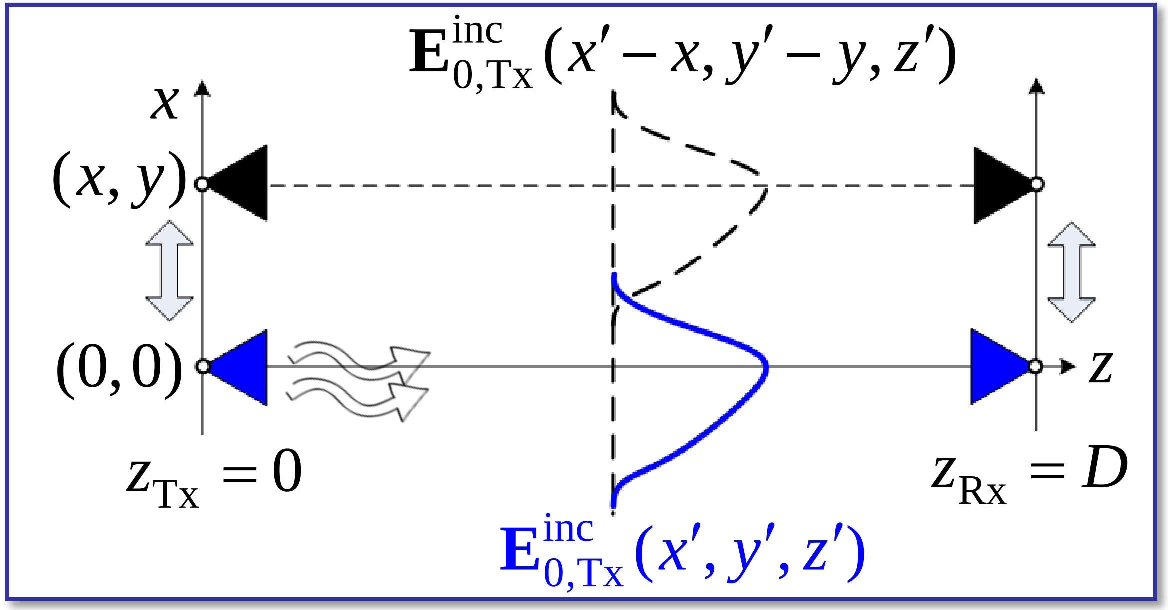

$$\Rightarrow S_\xi^{\text{sc}}(x,y,\overline{z};\omega) \approx \iiint_{V_s} \Delta\varepsilon_r(x',y',z')\mathcal{K}_{0,\xi}(x'-x,y'-y;z';\omega)dx'dy'dz'$$

HOLOGRAPHY: RESOLVENT KERNEL, examples

- **examples:** analytical kernels used with far-zone reflection data $(\bar{\mathbf{E}}^{\text{inc}}_{\xi,\text{Rx}} = \bar{\mathbf{E}}^{\text{inc}}_{\xi,\text{Tx}})$

plane waves: $\mathcal{K}_\xi(x',y',z';x,y,z_{\text{Rx}};\omega) = \bar{\mathbf{E}}^{\text{inc}}_{\text{Rx}} \cdot \bar{\mathbf{E}}^{\text{inc}}_{\text{Rx}} \sim e^{-\mathrm{i}2k_{\text{b}}\sqrt{(x-x')^2+(y-y')^2+(z-z')^2}}$

spherical waves: $\mathcal{K}_\xi(x',y',z';x,y,z_{\text{Rx}};\omega) \sim \dfrac{e^{-\mathrm{i}2k_{\text{b}}\sqrt{(x-x')^2+(y-y')^2+(z-z')^2}}}{(x-x')^2+(y-y')^2+(z-z')^2}$

cylindrical waves: $H_0^{(2)}(2k\rho),\ \rho = \sqrt{(x-x')^2+(y-y')^2},\ \ z = z' = const$

- **far-field analytical kernels** do not work well with near-field data

- **kernels computed from simulated incident-field distributions** suffer from modeling errors **[Amineh *et al*, *Trans. AP*, 2011]**

- **near-field kernels** are best determined through measuring the system PSF
[Savelyev&Yarovoy, *EuRAD* 2012][Amineh *et al*., *IEEE Trans. Instr.&Meas.*, 2015]

- PSF-based kernels enable **quantitative imaging in real time**

- PSF is the system response to a point scatterer

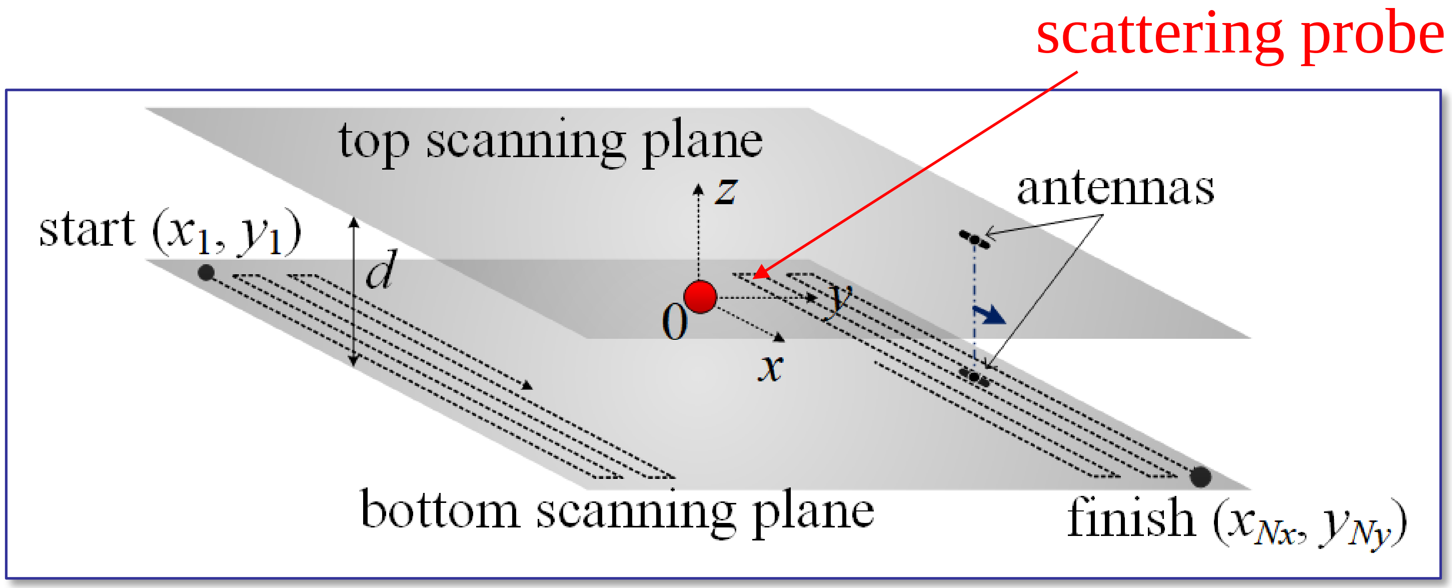

- relating PSF to kernel

Let $\text{PSF}_{0z',\xi}(x, y, \bar{z}; \omega) \equiv$

$$\text{PSF}_{\xi}(x, y, \bar{z}; \underbrace{0, 0, z'}_{\substack{\text{probe at center} \\ \text{of plane } z'=const}}; \omega)$$

Then $\mathcal{K}_{0,\xi}(x, y; z'; \omega) = \text{PSF}_{0z',\xi}(-x, -y, \bar{z}; \omega) / \left(\Delta\varepsilon_{r,\text{sp}} \Omega_{\text{sp}}\right)$

DATA EQUATION OF HOLOGRAPHY IN TERMS OF PSF

- in real space

$$S_{\xi}^{\mathrm{sc}}(x,y,\overline{z};\omega) \approx \frac{1}{\Delta\varepsilon_{r,\mathrm{sp}}\Omega_{\mathrm{sp}}} \int_{z'} \underbrace{\iint_{y'x'} \Delta\varepsilon_r(x',y',z') \cdot \mathrm{PSF}_{0z',\xi}(x-x',y-y';\omega)dx'dy'}_{\text{2D convolution}}\,dz'$$

- in Fourier (or k) space

$$\tilde{S}_{\xi}^{\mathrm{sc}}(k_x,k_y;\overline{z};\omega) \approx \frac{\Delta x'\Delta y'}{\Delta\varepsilon_{r,\mathrm{sp}}\Omega_{\mathrm{sp}}} \int_{z'} \underbrace{\tilde{F}(k_x,k_y;z')}_{\mathrm{FT}_{2\mathrm{D}}\{\Delta\varepsilon_r(x',y',z')\}} \cdot \widetilde{\mathrm{PSF}}_{0z',\xi}(k_x,k_y;\omega)\,dz'$$

- system of equations to solve ***at each spectral position*** $\boldsymbol{\kappa} = (k_x,k_y)$

$$\boxed{\tilde{S}_{\xi}^{(m)}(\boldsymbol{\kappa}) \approx \sum_{n=1}^{N_z} \tilde{f}(\boldsymbol{\kappa};z_n')\widetilde{\mathrm{PSF}}_{0z',\xi}^{(m)}(\boldsymbol{\kappa})} \qquad \begin{aligned} m &= 1,\ldots,N_{\omega} \\ \xi &= 1,\ldots,N_T \end{aligned}$$

$$\tilde{f}(\boldsymbol{\kappa};z_n') = \frac{\overbrace{\boxed{\Delta x'\Delta y'\Delta z_n'}}^{\Omega_{\mathrm{v}}}}{\Delta\varepsilon_{r,\mathrm{sp}}\Omega_{\mathrm{sp}}} \cdot \tilde{F}(\boldsymbol{\kappa};z_n')$$

ADVANTAGES OF SOLVING IN FOURIER SPACE: *DIVIDE AND CONQUER*

$$\boxed{\tilde{S}_{\xi}^{(m)}(\boldsymbol{\kappa}_{ij}) \approx \sum_{n=1}^{N_z} \tilde{f}(\boldsymbol{\kappa}_{ij}; z'_n)\widetilde{\mathrm{PSF}}_{0z',\xi}^{(m)}(\boldsymbol{\kappa}_{ij})} \qquad \begin{array}{l} m = 1,\ldots,N_\omega \\ \xi = 1,\ldots,N_T \end{array}$$

$$\Rightarrow \quad \boxed{\mathbf{A}(\boldsymbol{\kappa}_{ij})_{[N_T N_\omega \times N_z]} \cdot \mathbf{f}(\boldsymbol{\kappa}_{ij})_{[N_z \times 1]} = \mathbf{d}(\boldsymbol{\kappa}_{ij})_{[N_T N_\omega \times 1]}} \qquad \begin{array}{l} \boldsymbol{\kappa}_{ij} = (i\Delta k_x, j\Delta k_y) \\ i = 1,\ldots,N_x; \;\; j = 1,\ldots,N_y \end{array}$$

- we solve ($N_x \cdot N_y$) such systems (on the order of 10^4 to 10^5)
- the size of each system is small: $N_T N_\omega \times N_z$ (e.g. 60×5)
- **typical execution times: 2 to 3 seconds on a laptop using Matlab**
- solution is orders of magnitude faster than solving in real space:

$$N_D \times N_\mathrm{v} \text{ where } \begin{array}{l} N_\mathrm{v} = N_x N_y N_z \sim 10^6 \text{ to } 10^7 \\ N_D = N_x N_y N_\omega N_T \sim 10^7 \text{ to } 10^8 \end{array}$$

FINAL STEP: BACK TO REAL SPACE

- at each plane along range ($z' = const$)

$$\Delta\varepsilon_r(x', y', z_n') = \frac{\Delta\varepsilon_{r,\mathrm{sp}}\Omega_{\mathrm{sp}}}{\Delta x' \Delta y' \Delta z_n'} \mathcal{F}_{\mathrm{2D}}^{-1}\left\{ \tilde{f}(\boldsymbol{\kappa}; z_n') \right\}, \; n = 1, \ldots, N_z$$

$$\varepsilon_r(x', y', z_n') = \varepsilon_{r,\mathrm{b}} + \Delta\varepsilon_r(x', y', z_n')$$

EXAMPLE: METALLIC TARGETS IN AIR

[Amineh *et al.*, *Trans. Instr.&Meas.*, 2015]

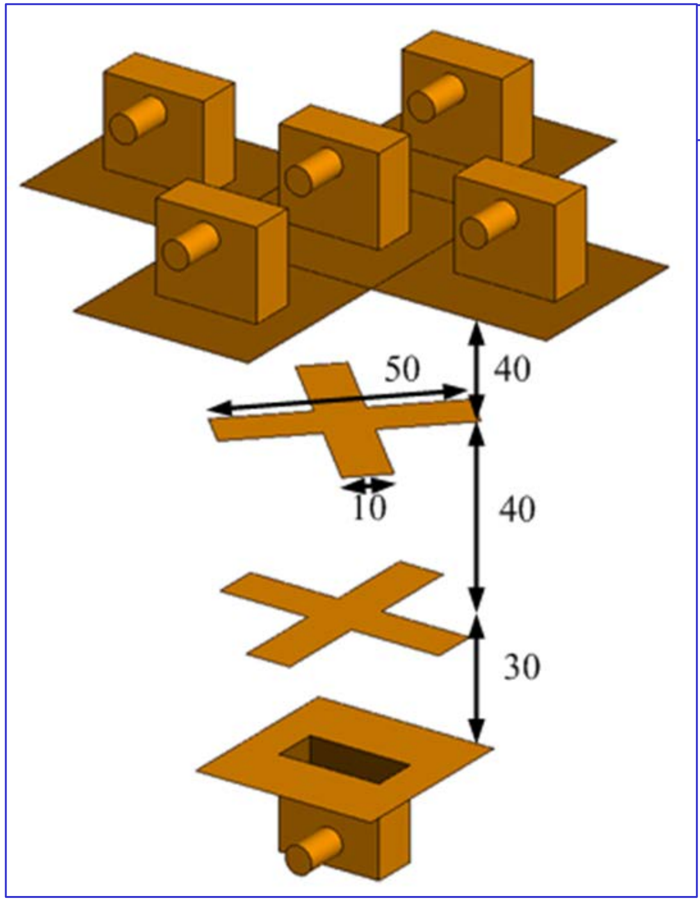

$\Delta x = \Delta y = 5\,\text{mm}$
$\Delta f = 250\,\text{MHz}$

f (GHz)	λ (mm)	D_{far} (mm)
3	100	12.5
8.2	37	34
20	15	83

X-band (WR90) open-end waveguides ($f_c \approx 6.56\,\text{GHz}$)

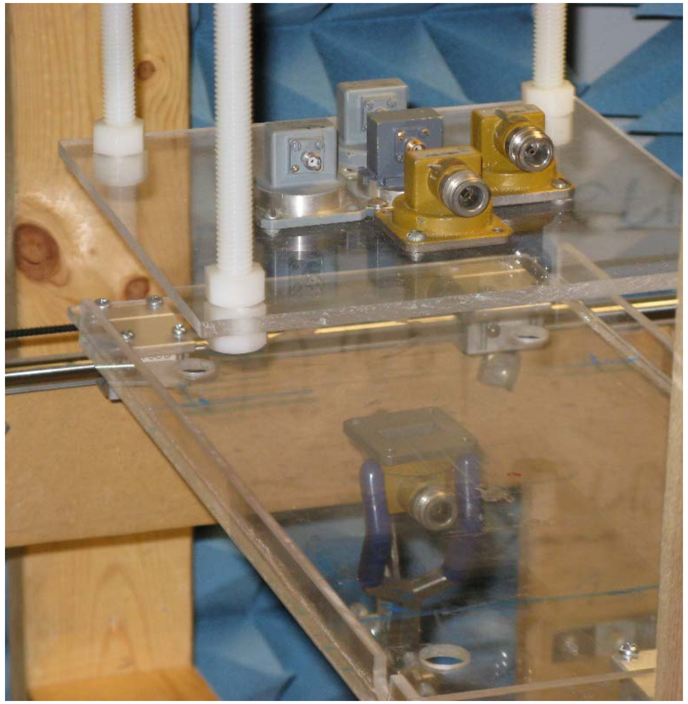

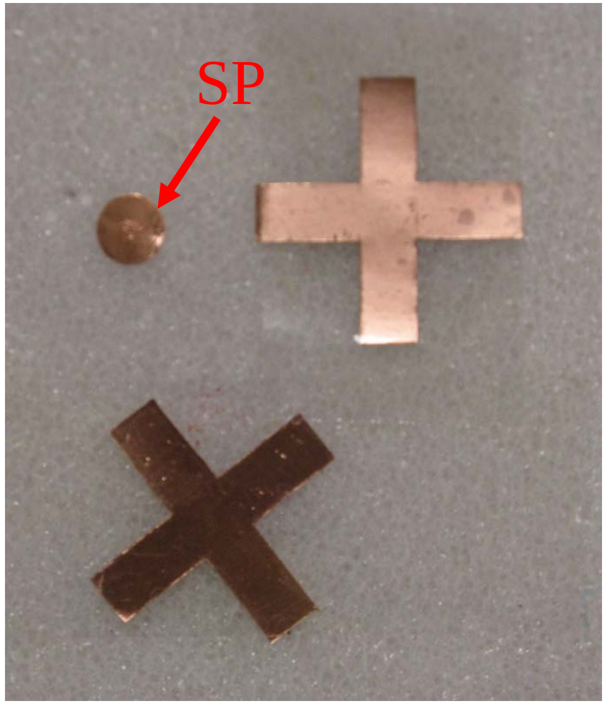

[photo credit: Justin McCombe]

METALLIC TARGETS IN AIR – RESULTS WITH SIMULATED KERNELS

[Amineh *et al.*, *Trans. Instr.&Meas.*, 2015]

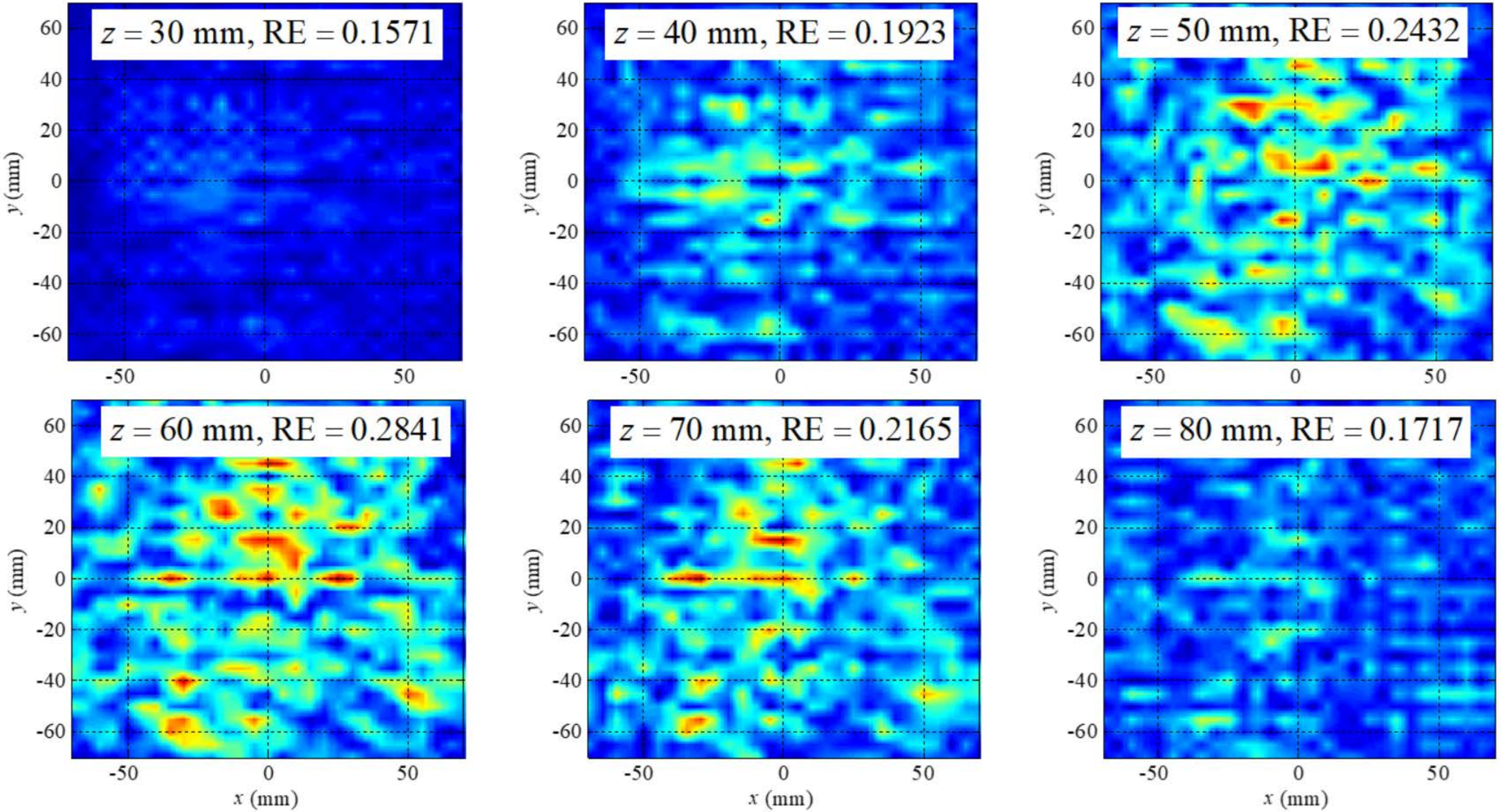

METALLIC TARGETS IN AIR – RESULTS WITH MEASURED KERNELS (PSF)

[Amineh *et al.*, *Trans. Instr.&Meas.*, 2015]

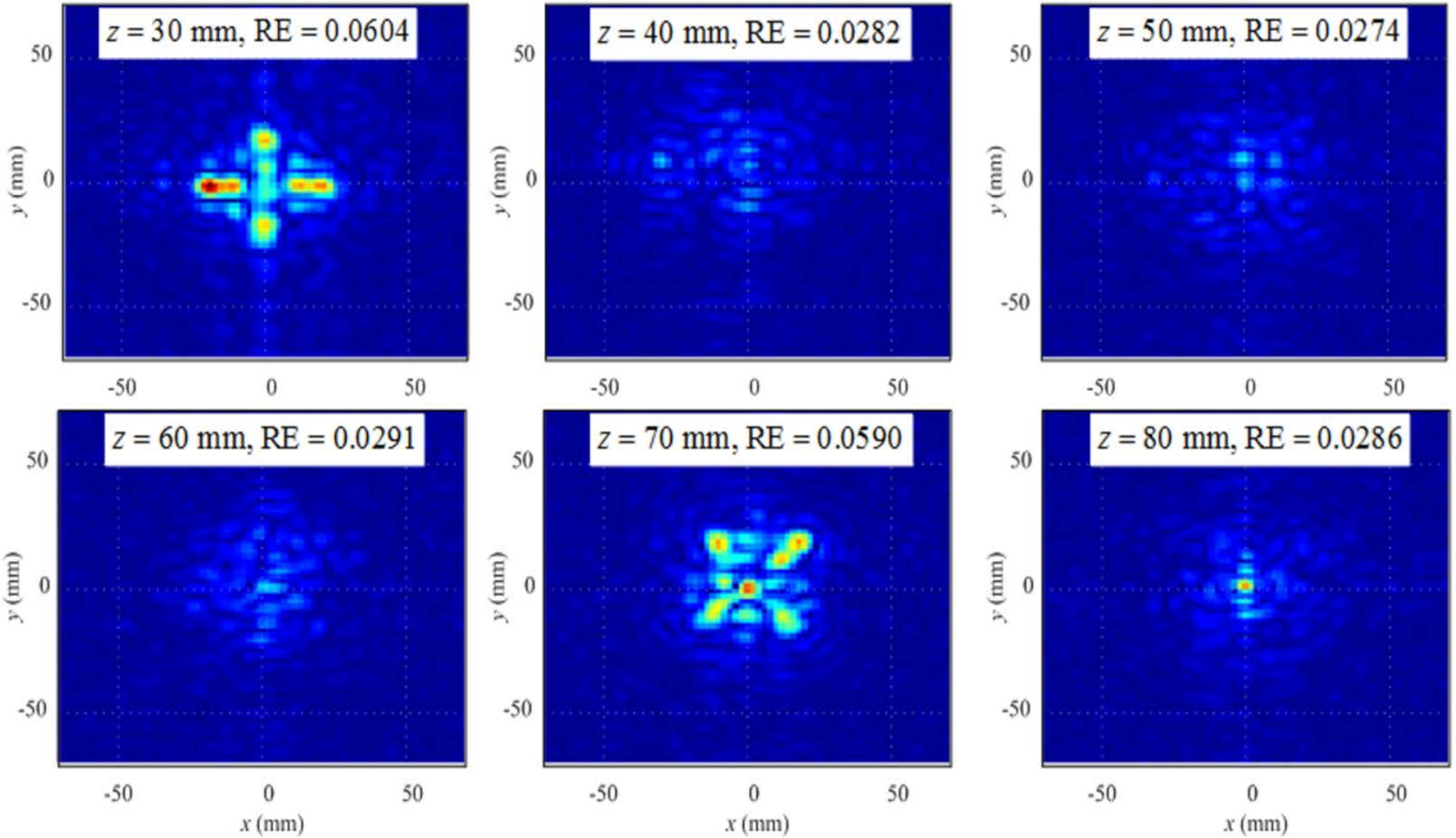

expected spatial resolution

depth:
$\delta_z \approx 10$ mm

lateral:
$\delta_{x,y} \approx 4$ mm

EXAMPLE: IMAGING TISSUE

[Tajik *et al.*, *JPIER-B* 2017]

[photo credit: Daniel Tajik]

a layer in the OUT

Tissue	Color Highlight	Relative Permittivity Averaged over 3 to 8 GHz
Chicken Wing	red	NA
Bone	green	21 – 10i
Skin	yellow	13 – 6i
Muscle	blue	45 – 23i
Peanut Butter & Jam	brown	7 – 3i
Carbon Rubber	black	10 – 3i

$$\Delta x = \Delta y = 3\,\text{mm}$$
$$\Delta f = 100\,\text{MHz}$$
$$f \in [3,8]\ \text{GHz}$$

EXAMPLE: IMAGING TISSUE

[Tajik *et al.*, *JPIER-B* 2017]

[photo credit: Daniel Tajik]

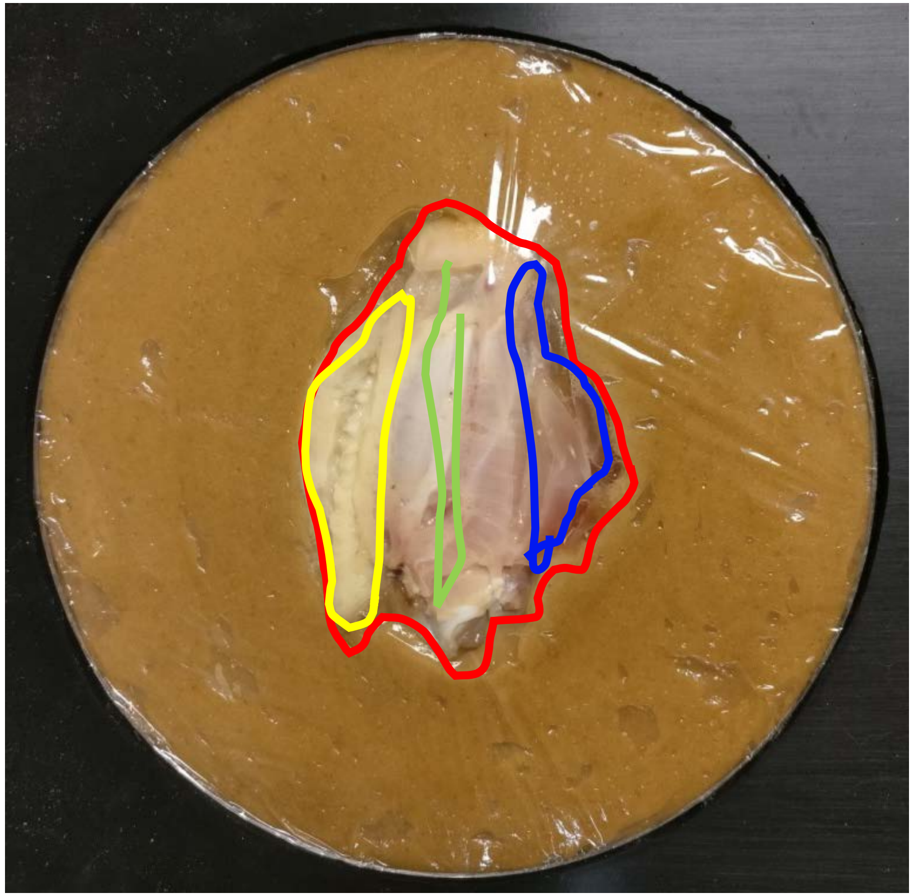

a layer in the OUT

Tissue	Color Highlight	Relative Permittivity Averaged over 3 to 8 GHz
Chicken Wing	red	NA
Bone	green	21 – 10i
Skin	yellow	13 – 6i
Muscle	blue	45 – 23i
Peanut Butter & Jam	brown	7 – 3i
Carbon Rubber	black	10 – 3i

$$\Delta x = \Delta y = 3\,\mathrm{mm}$$
$$\Delta f = 100\,\mathrm{MHz}$$
$$f \in [3,8]\ \mathrm{GHz}$$

EXAMPLE: ACQUIRING THE PSF

[Tajik *et al.*, *JPIER-B* 2017]

[photo credit: Daniel Tajik]

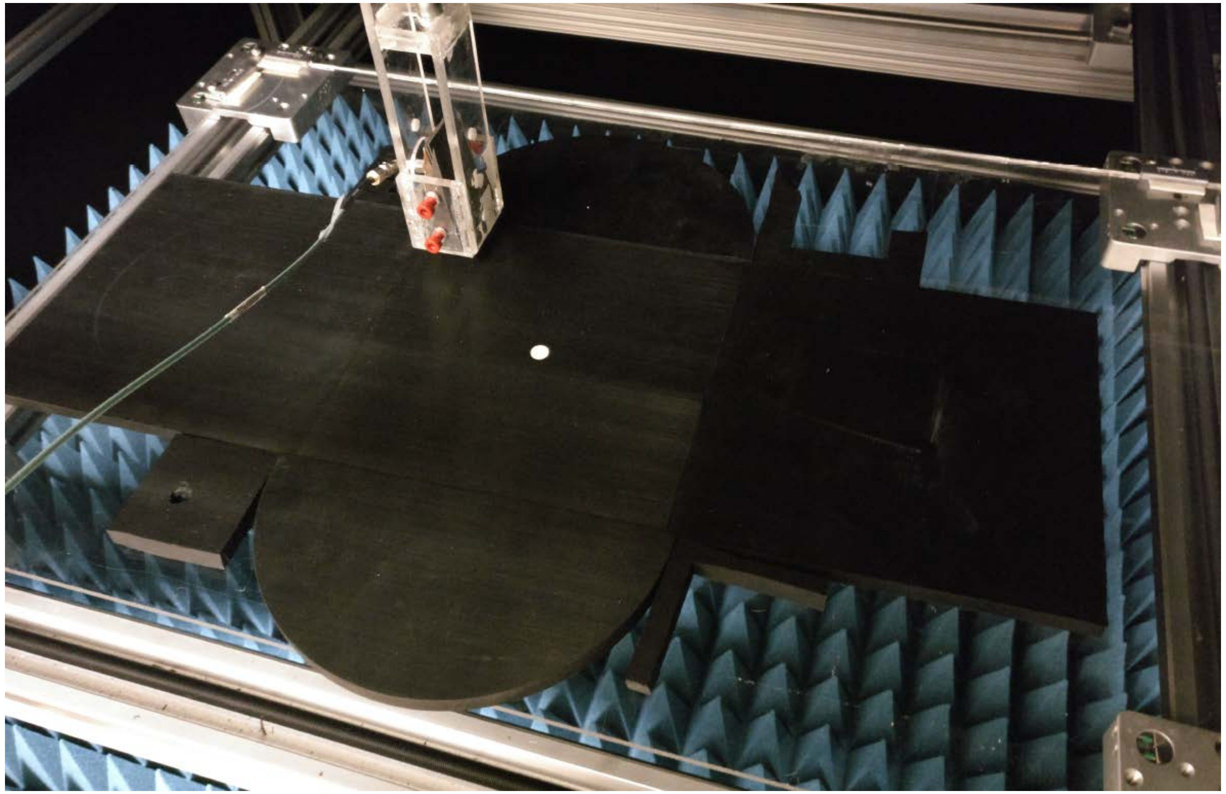

calibration object with small scattering probe
at center: $\varepsilon_{r,\mathrm{SP}} \approx 18 - \mathrm{i}0,$ radius 5 mm, height 10 mm

EXAMPLE: IMAGING TISSUE

[Tajik *et al.*, *JPIER-B* 2017][*EuCAP* 2018]

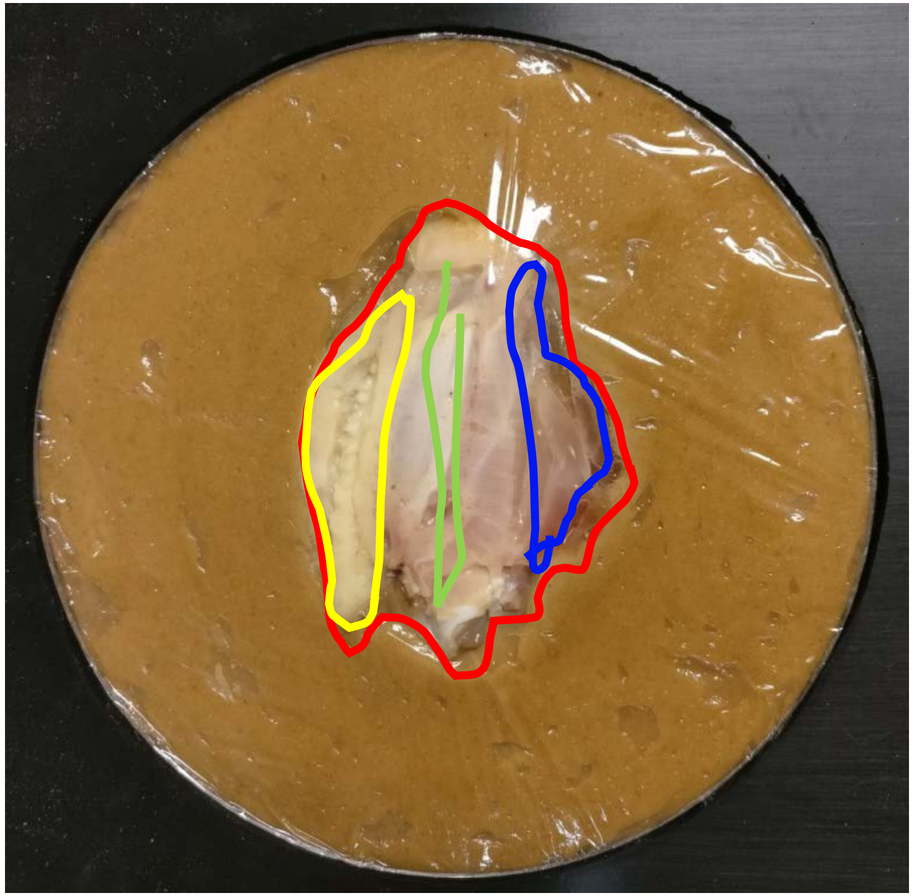

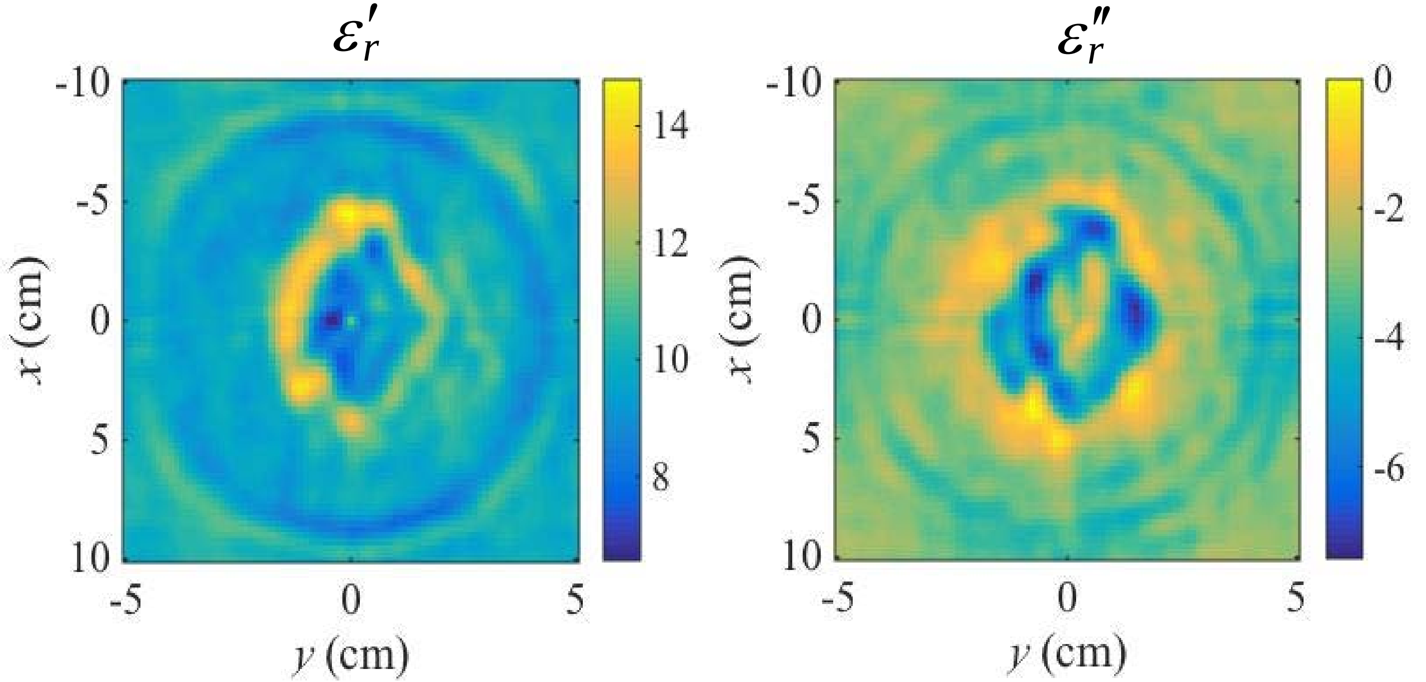

QUALITATIVE IMAGING WITH **SENSITIVITY MAPS**

[Tu *et al.*, *Inv. Problems*, 2015]

- reconstruction formula

$$D(\mathbf{r}') = \sum_{\xi=1}^{N_T} \int_\omega \iint_{\mathbf{r}\in S_a} \underbrace{\left[S_\xi^{\text{inc}} - S_\xi^{\text{tot}} \right]_{(\mathbf{r},\omega)}}_{\approx - S_\xi^{\text{sc}}(\mathbf{r},\omega)} \cdot \left[\frac{\partial S_\xi^{\text{inc}}(\mathbf{r},\omega)}{\partial \varepsilon(\mathbf{r}')} \right]^* d\mathbf{r}\, d\omega$$

adjoint sensitivity formula using simulated incident fields

- sensitivity map: 3D image of Fréchet derivative of ℓ_2 norm of the differences of all total and incident responses

$$D(\mathbf{r}') = \mathcal{J}\left\{F[\varepsilon(\mathbf{r}')]\right\} = 0.5 \sum_{\xi=1}^{N_T} \int_\omega \iint_{\mathbf{r}\in S_a} \left\| S_\xi^{\text{tot}}(\mathbf{r},\omega) - S_\xi^{\text{inc}}[\mathbf{r},\omega;\varepsilon(\mathbf{r}')] \right\|_2^2 d\mathbf{r}\, d\omega$$

$$\operatorname{Re}\left\{ D^{(m)}(\mathbf{r}') \right\} = \frac{dF^{(m)}}{d\varepsilon'(\mathbf{r}')}$$ $\rightarrow$ indicates where contrast in ε' exists

$$\operatorname{Im}\left\{ D^{(m)}(\mathbf{r}') \right\} = -\frac{dF^{(m)}}{d\varepsilon''(\mathbf{r}')}$$ $\rightarrow$ indicates where contrast in ε'' exists

SENSITIVITY MAPS USING MEASURED PSFs: THE NEAR-FIELD CASE

- from simulated incident fields to measured PSFs

$$\frac{\partial S_{\xi}^{\text{inc}}(\mathbf{r},\omega)}{\partial\varepsilon(\mathbf{r}')} \approx \frac{\Delta S_{\xi}^{\text{inc}}(\mathbf{r},\omega)}{\Delta\varepsilon(\mathbf{r}')} \approx \frac{\bar{S}_{\xi,\text{sp}}^{\text{tot}}(\mathbf{r},\omega) - S_{\xi}^{\text{inc}}(\mathbf{r},\omega)}{\Delta\varepsilon_{\text{sp}}(\mathbf{r}')} = \frac{\text{PSF}_{\xi}^{\text{sc}}(\mathbf{r},\omega;\mathbf{r}')}{\Delta\varepsilon_{\text{sp}}}$$

scattering probe at r'

$$\text{PSF}_{\xi}^{\text{sc}}(x,y,\bar{z},\omega;x',y',\bar{z}') = \text{PSF}_{\xi,0}^{\text{sc}}(x-x',y-y',\bar{z},\omega;\bar{z}')$$

scattering probe at center of z' plane

uniform background along *x* and *y*

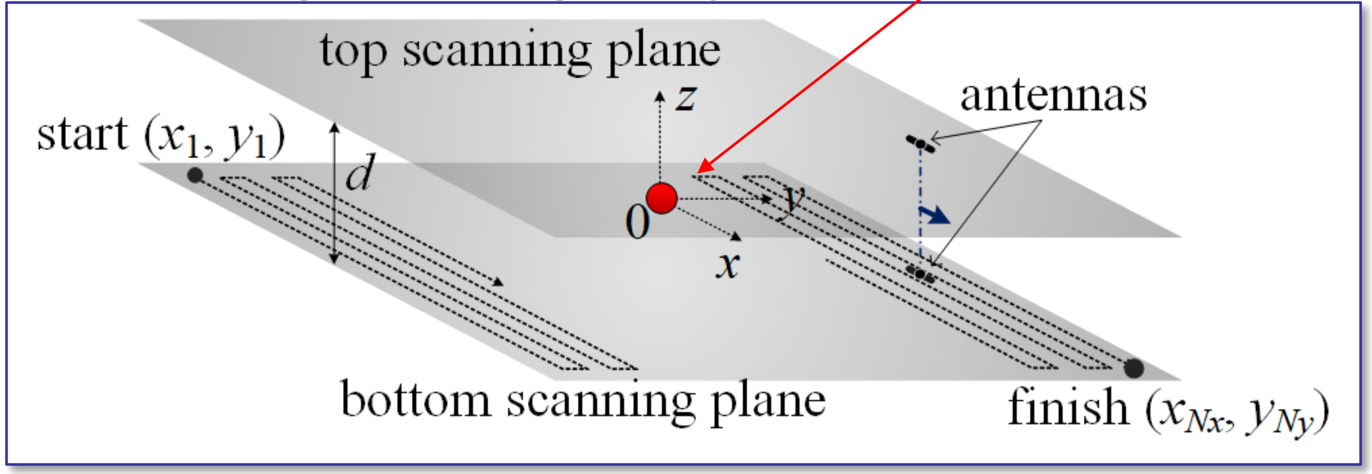

SENSITIVITY MAPS USING MEASURED PSFs: THE NEAR-FIELD CASE – 2

[Nikolova, *Introduction to Microwave Imaging*, 2017][Shumakov *et al.*, *IEEE Trans. MTT*, 2018]

- sensitivity reconstruction formula with PSFs: ***scattered-power maps (SPM)***

$$-\Delta\varepsilon_{\text{sp}} \cdot D(\mathbf{r}') = \boxed{M(\mathbf{r}') = \sum_{\xi=1}^{N_T} \int_\omega \iint_{\mathbf{r}\in S_{\text{a}}} S_\xi^{\text{sc}}(\mathbf{r},\omega) \cdot \left[\text{PSF}_{\xi,0}^{\text{sc}}(\mathbf{r},\omega;\mathbf{r}')\right]^* d\mathbf{r}\, d\omega}$$

- SPM reconstruction formula with planar scanning

$$M^{(m)}(x',y',\overline{z}') = \sum_{\xi=1}^{N_T} \int_\omega \underbrace{\iint_{S_{\text{a}}} \left[S_\xi^{\text{sc}}(x,y,\overline{z},\omega)\right] \cdot \left[\text{PSF}_\xi^{\text{sc}}\left(x-x',y-y',\overline{z},\omega;\overline{z}'\right)\right]^* dxdy}_{\text{cross-correlation of response } S_\xi^{\text{sc}} \text{ and } \text{PSF}_\xi^{\text{sc}} \text{ in } (x,y)}\, d\omega$$

- reconstruction is practically instantaneous – no systems of equations are solved
- effort shifted to near-field system calibration – measuring PSFs or simulating incident fields to compute response sensitivity $\partial S_\xi^{\text{inc}}(\mathbf{r},\omega) / \partial\varepsilon(\mathbf{r}')$

SCATTERED-POWER MAPS: SIMULATION EXAMPLE (*Altair FEKO*)

simulation of PSF acquisition

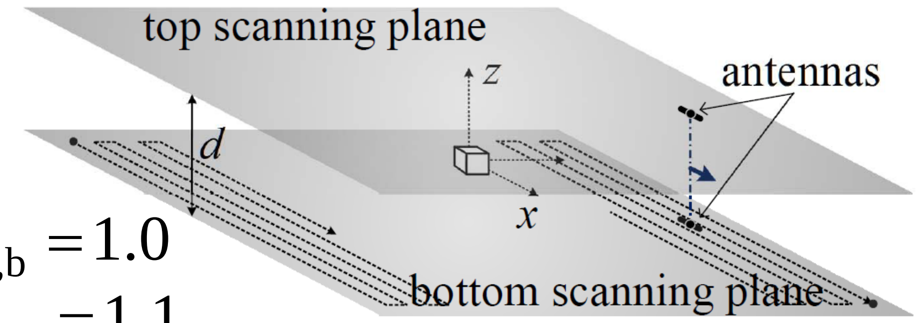

$\varepsilon_{r,b} = 1.0$
$\varepsilon_{r,sp} = 1.1$

simulation of data acquisition

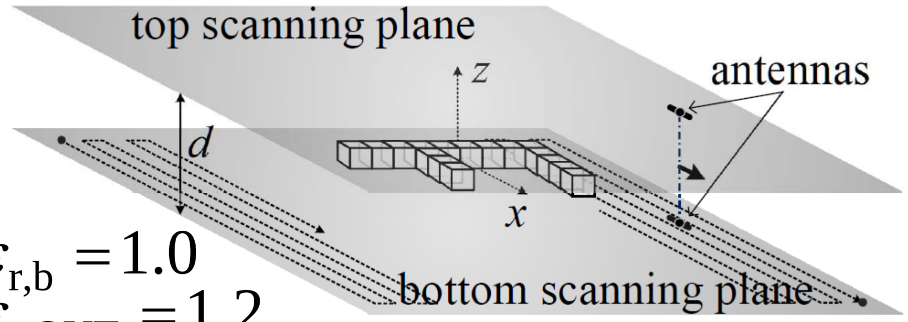

$\varepsilon_{r,b} = 1.0$
$\varepsilon_{r,OUT} = 1.2$

sample PSF: S_{11} at 4 GHz MAG/PHASE

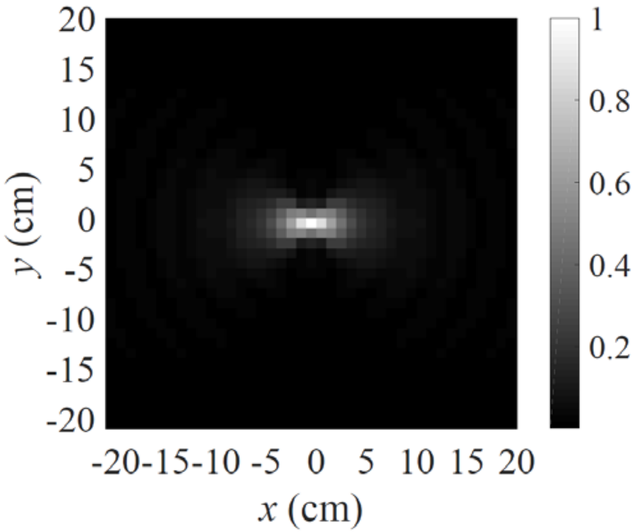

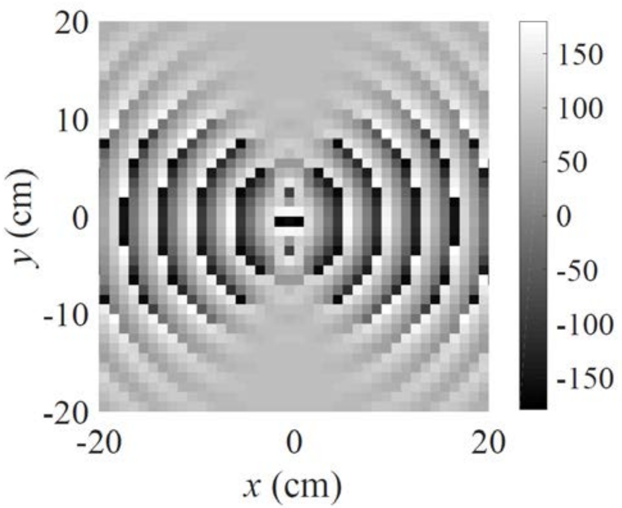

$f_{min} = 3$ GHz
$f_{max} = 16$ GHz
$\Delta f = 1$ GHz

SCATTERED-POWER MAPS: SIMULATION EXAMPLE (F SHAPE)

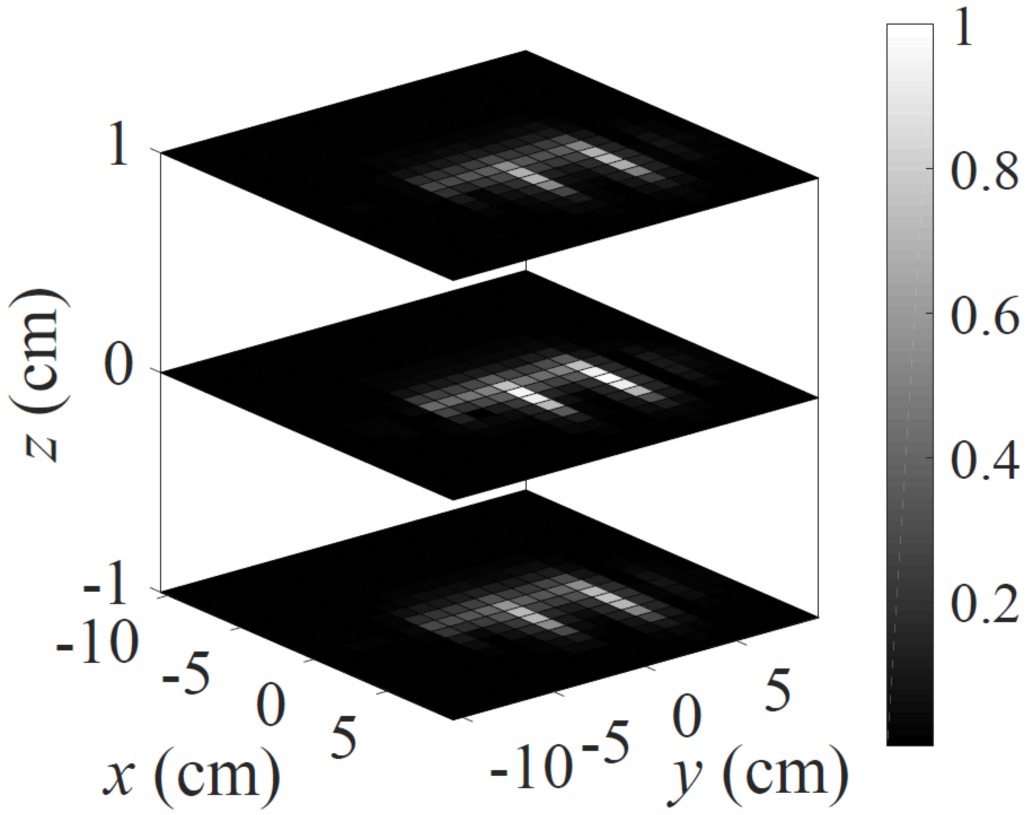

- blurring typical for cross-correlation methods – diffraction limit, limited number of responses

QUANTITATIVE REAL-TIME IMAGING WITH SPM

[Tu *et al.*, *Inv. Problems*, 2015][Shumakov *et al.*, *IEEE Trans. MTT*, 2018]

- requires measured PSFs – they scale accurately with the scattering-probe contrast
- reconstruction solves the linear problem

$$\underbrace{M(\mathbf{r}')}_{\text{qualitative image (SPM) of OUT}} = \frac{1}{\Delta\varepsilon_{\mathrm{r,sp}}\Omega_{\mathrm{sp}}} \iiint_{V_s} \underbrace{\Delta\varepsilon_{\mathrm{r}}(\mathbf{r}'')}_{\text{unknown contrast}} \underbrace{M_{\mathrm{sp@}\mathbf{r}''}(\mathbf{r}')}_{\text{qualitative image (SPM) of scattering probe}} d\mathbf{r}''$$

- real-time solution via inversion in Fourier space (similar to holography)

$$M(x',y',z') = \frac{1}{\Delta\varepsilon_{\mathrm{r,sp}}\Omega_{\mathrm{sp}}} \int_{z''} \underbrace{\int_{y''}\int_{x''} \Delta\varepsilon_{\mathrm{r}}(x'',y'',z'') \cdot M_{\mathrm{sp@}(0,0,z'')}(x'-x'', y'-y'', z')\, dx''dy''}_{\text{convolution in } (x,y)}\, dz''$$

QUANTITATIVE REAL-TIME IMAGING WITH SPM: FOURIER SPACE SOLUTION

$$\tilde{M}(k_x, k_y, z_p) = \frac{\Omega_\text{v}}{\Delta\varepsilon_\text{r,sp}\Omega_\text{sp}} \sum_{q=1}^{N_z} \tilde{f}(k_x, k_y, z_q) \cdot \tilde{M}_{\text{sp@}(0,0,z_q)}(k_x, k_y, z_p), \;\; p = 1, \ldots, N_z$$

- small square system of equations to solve ***at each spectral position*** $\boldsymbol{\kappa} = (k_x, k_y)$

$$\boxed{\boldsymbol{M}_{(\boldsymbol{\kappa})} \boldsymbol{x}_{(\boldsymbol{\kappa})} = \boldsymbol{m}_{(\boldsymbol{\kappa})}}$$

$$\boldsymbol{x}_{(\boldsymbol{\kappa})} = \left[\tilde{f}(\boldsymbol{\kappa}, z_1) \cdots \tilde{f}(\boldsymbol{\kappa}, z_{N_z}) \right]^T$$

$$\boldsymbol{m}_{(\boldsymbol{\kappa})} = \left[\tilde{M}(\boldsymbol{\kappa}, z_1) \cdots \tilde{M}(\boldsymbol{\kappa}, z_{N_z}) \right]^T$$

$$\boldsymbol{M}_{(\boldsymbol{\kappa})} = \begin{bmatrix} \tilde{M}_{\text{sp@}(0,0,z_1)}(\boldsymbol{\kappa}, z_1) & \cdots & \tilde{M}_{\text{sp@}(0,0,z_{N_z})}(\boldsymbol{\kappa}, z_1) \\ \vdots & \ddots & \vdots \\ \tilde{M}_{\text{sp@}(0,0,z_1)}(\boldsymbol{\kappa}, z_{N_z}) & \cdots & \tilde{M}_{\text{sp@}(0,0,z_{N_z})}(\boldsymbol{\kappa}, z_{N_z}) \end{bmatrix}$$

- final step: back to (x,y) space

$$\Delta\varepsilon_r(x', y', z'_n) = \frac{\Delta\varepsilon_{r,\text{sp}}\Omega_\text{sp}}{\Omega_\text{v}} \mathcal{F}_\text{2D}^{-1}\left\{ \tilde{f}(\boldsymbol{\kappa}; z'_n) \right\}, \; n = 1, \ldots, N_z$$

QUANTITATIVE SPM: SIMULATION EXAMPLE (F SHAPE)

[Nikolova, *Introduction to Microwave Imaging*, 2017]

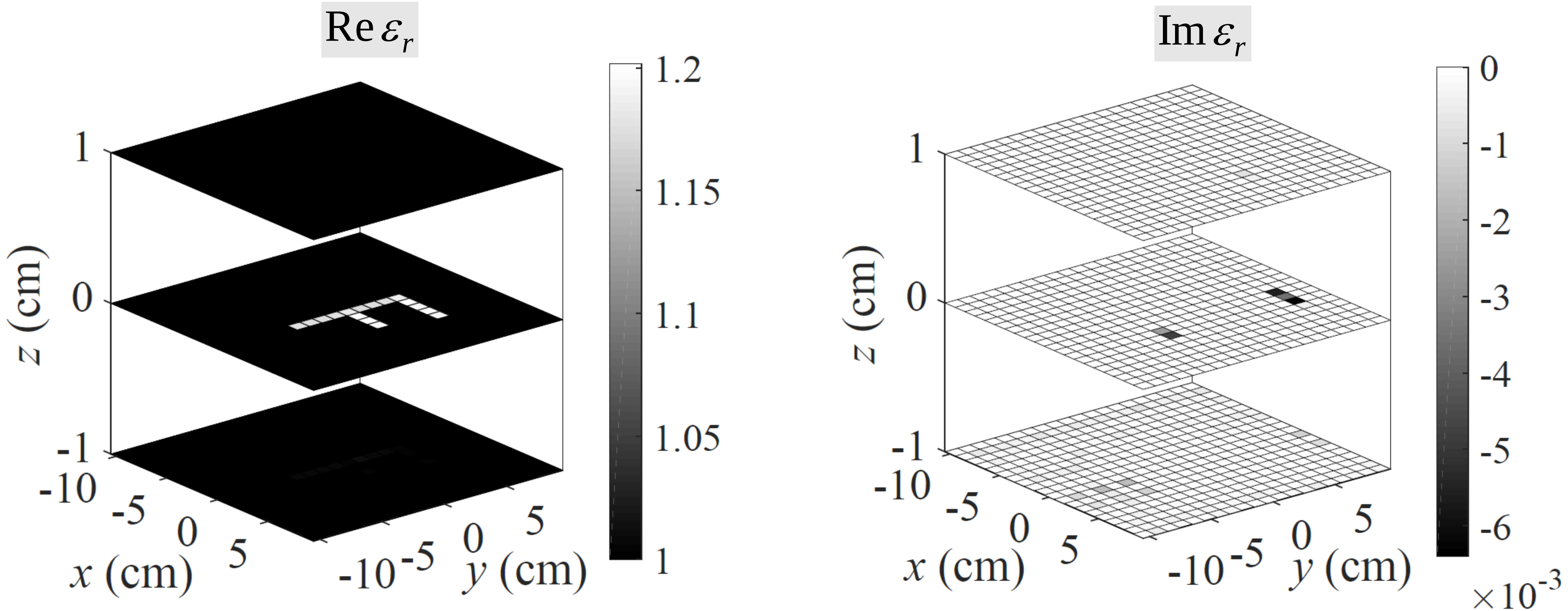

QUANTITATIVE SPM: EXPERIMENTAL EXAMPLE

[Shumakov *et al.*, *IEEE Trans. MTT*, 2018]

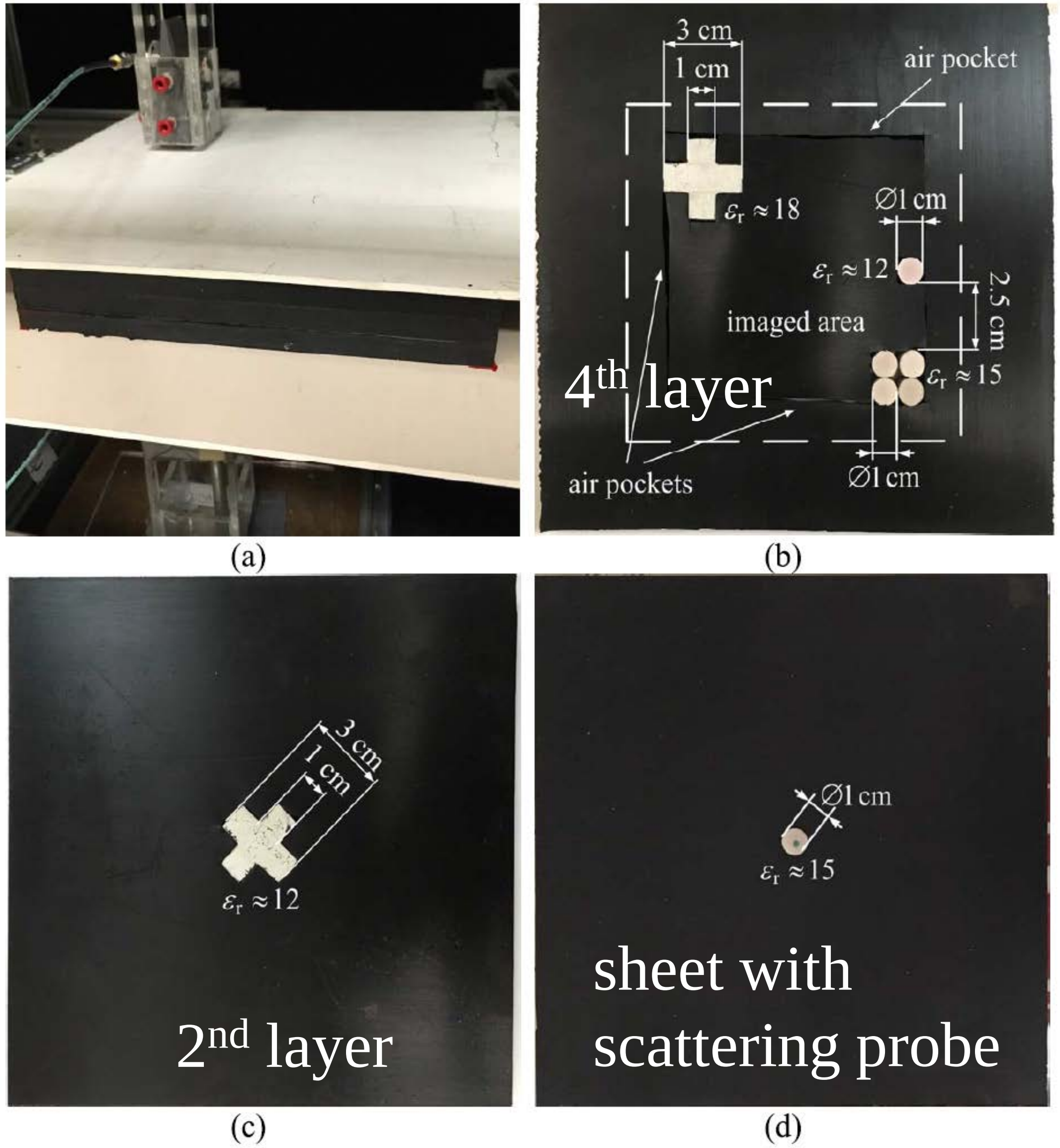

5 cm thick carbon-rubber sample $\varepsilon_{r,\mathrm{b}} \approx 10 - \mathrm{i}5$

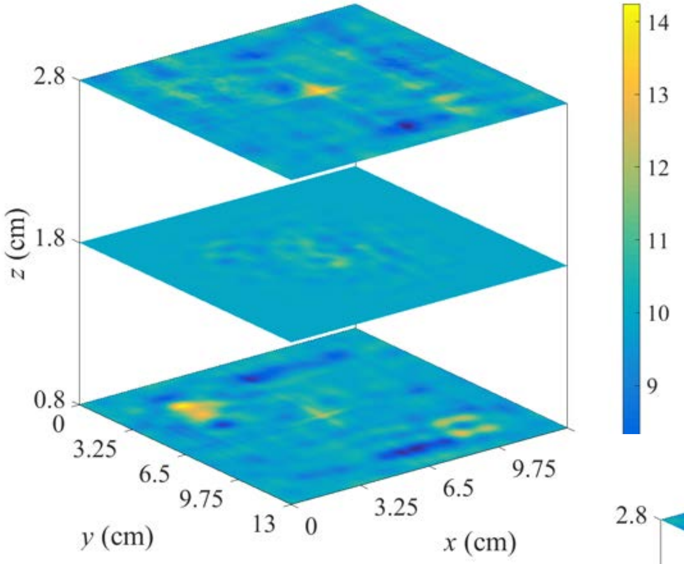

$\mathrm{Re}\,\varepsilon_r$

$\mathrm{Im}\,\varepsilon_r$

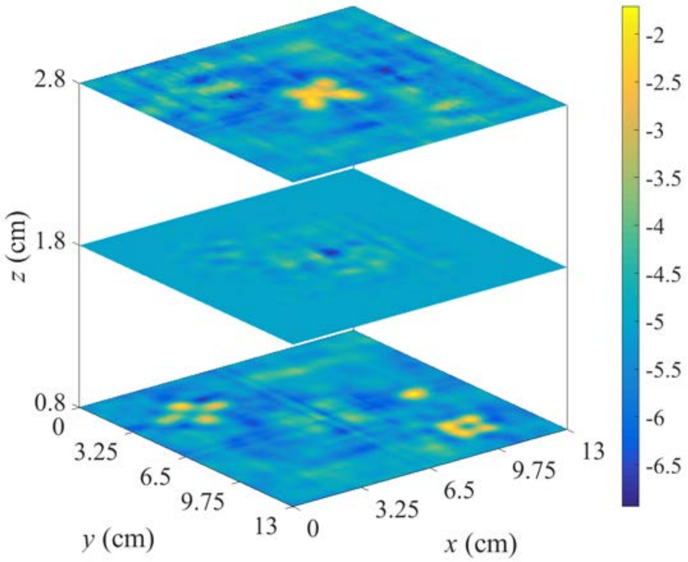

TIME DOMAIN FORWARD MODEL WITH PSF

[Nikolova, *Introduction to Microwave Imaging*, 2017]

- linearized time-domain resolvent kernel

$$s^{\mathrm{sc}}(\mathbf{r},t) \approx \iiint_{V_s} \kappa(\mathbf{r}') \Big[h_{\mathrm{Rx}}^{\mathrm{inc}} * \underbrace{h_{\mathrm{Tx}}^{\mathrm{inc}} * w''}_{(u_{\mathrm{Tx}}^{\mathrm{inc}})''} \Big]_{(\mathbf{r}';\mathbf{r},t)} d\mathbf{r}'$$

$$\kappa(\mathbf{r}') = \frac{\Delta\varepsilon_r}{v_{\mathrm{b}}^2}$$

$$\Rightarrow \mathcal{K}(\mathbf{r}';\mathbf{r},t) = h_{\mathrm{Rx}}^{\mathrm{inc}}(\mathbf{r}';\mathbf{r}_{\mathrm{Rx}},t) * h_{\mathrm{Tx}}^{\mathrm{inc}}(\mathbf{r}';\mathbf{r}_{\mathrm{Tx}},t) * w''(t)$$

- resolvent kernel and PSF all over again:

  measure response with each antenna pair and position of a point scatterer at $\mathbf{r}' = 0$

$$\mathrm{PSF}_0(\mathbf{r}_{\mathrm{Rx}},\mathbf{r}_{\mathrm{Tx}},t) = \kappa_{\mathrm{sp}}\Omega_{\mathrm{sp}} \Big[h_{\mathrm{Rx}}^{\mathrm{inc}} * h_{\mathrm{Tx}}^{\mathrm{inc}} * w'' \Big]_{(\mathbf{r}'=0;\mathbf{r}_{\mathrm{Rx}},\mathbf{r}_{\mathrm{Tx}},t)}$$
$$= \kappa_{\mathrm{sp}}\Omega_{\mathrm{sp}} \mathcal{K}_0(\mathbf{r}_{\mathrm{Rx}},\mathbf{r}_{\mathrm{Tx}},t)$$

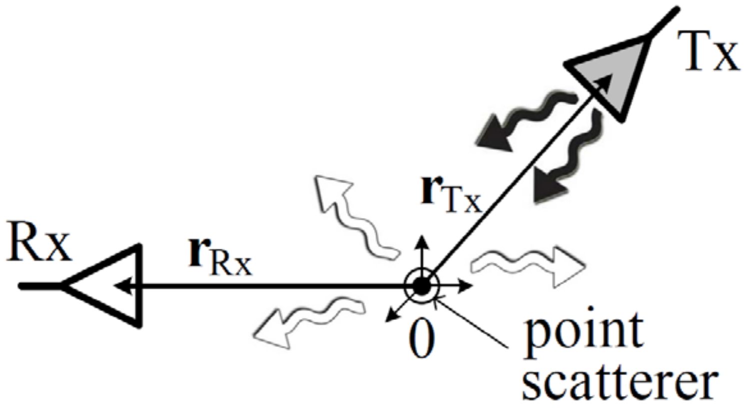

TIME DOMAIN FORWARD MODEL WITH PSF – 2

- assuming uniform background: $\mathcal{K}_{\mathbf{r}'}(\mathbf{r}_{\mathrm{Rx}},\mathbf{r}_{\mathrm{Tx}};t) \approx \mathcal{K}_0\left(\mathbf{r}_{\mathrm{Rx}},\mathbf{r}_{\mathrm{Tx}};t-\Delta t(\mathbf{r}')\right)$

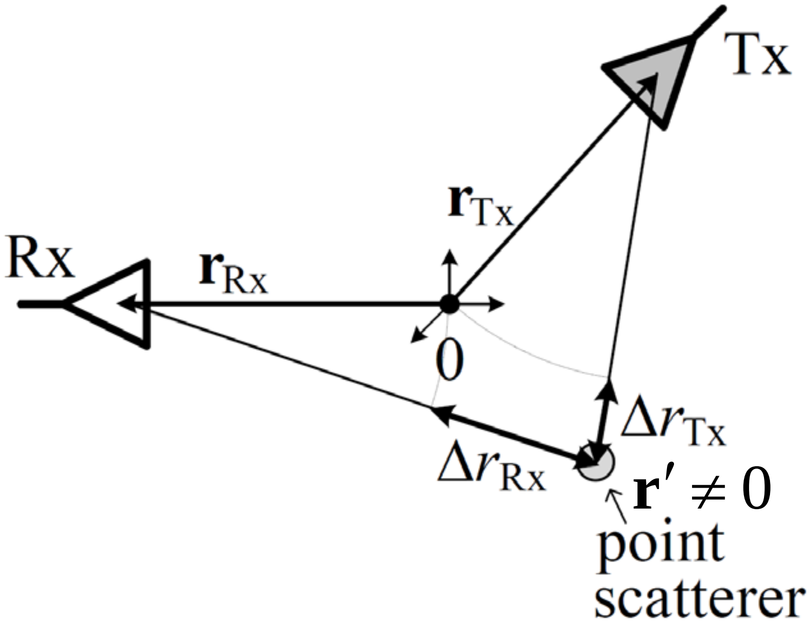

- example: analytical far-zone kernel

some reference time

$$\mathcal{K}_{\mathbf{r}'}(\underbrace{\mathbf{r}_{\mathrm{Rx}},\mathbf{r}_{\mathrm{Tx}}}_{\text{implied in }\mathbf{r}};t) \sim \mathrm{PSF}_0(\mathbf{r}_{\mathrm{Rx}},\mathbf{r}_{\mathrm{Tx}},t) \sim \delta\left(t-\frac{|\mathbf{r}'-\mathbf{r}_{\mathrm{Tx}}|}{v_{\mathrm{b}}}-\frac{|\mathbf{r}'-\mathbf{r}_{\mathrm{Rx}}|}{v_{\mathrm{b}}}-t_0\right)/\,r^2$$

DELAY AND SUM (DAS): THE CROSS-CORRELATION EXPLANATION

- cross-correlation – a measure of signal similarity

steering filter for antenna pair at **r** *toward voxel* **r**′

$$X(t,\mathbf{r}') = \sum_{\xi=1}^{N_T} \iint_{\mathbf{r}\in S_\mathrm{a}} \mathrm{PSF}_{\xi,0}(t,\mathbf{r},\mathbf{r}') \otimes s_\xi(t,\mathbf{r})\, d\mathbf{r}$$

⇦ *signal processing*

$$\sim \iiint_{\mathbf{r}''\in V_\mathrm{s}} \kappa(\mathbf{r}'') \cdot \sum_{\xi=1}^{N_T} \iint_{\mathbf{r}\in S_\mathrm{a}} \mathrm{PSF}_{\xi,0}(t,\mathbf{r},\mathbf{r}') \otimes \mathrm{PSF}_{\xi,0}(t,\mathbf{r},\mathbf{r}'')\, d\mathbf{r}\, d\mathbf{r}''$$

- with large number of responses, $X(\mathbf{r}',t) \sim \kappa(\mathbf{r}')$ as autocorrelation term dominates $\mathbf{r}''$ integral

autocorrelation term: $\kappa(\mathbf{r}') \cdot \sum_{\xi=1}^{N_T} \iint_{\mathbf{r}\in S_\mathrm{a}} \mathrm{PSF}_{\xi,0}(t,\mathbf{r},\mathbf{r}') \otimes \mathrm{PSF}_{\xi,0}(t,\mathbf{r},\mathbf{r}')\, d\mathbf{r}$

cross-correlation terms: $\kappa(\mathbf{r}'') \cdot \sum_{\xi=1}^{N_T} \iint_{\mathbf{r}\in S_\mathrm{a}} \mathrm{PSF}_{\xi,0}(t,\mathbf{r},\mathbf{r}') \otimes \mathrm{PSF}_{\xi,0}(t,\mathbf{r},\mathbf{r}'')\, d\mathbf{r}$

DAS: SIGNAL-FLOW SCHEMATIC

- image generation: plot the "intensity" distribution $I(\mathbf{r}') = \int_{t=0}^{T_{\max}} X^2(t,\mathbf{r}')\,dt$

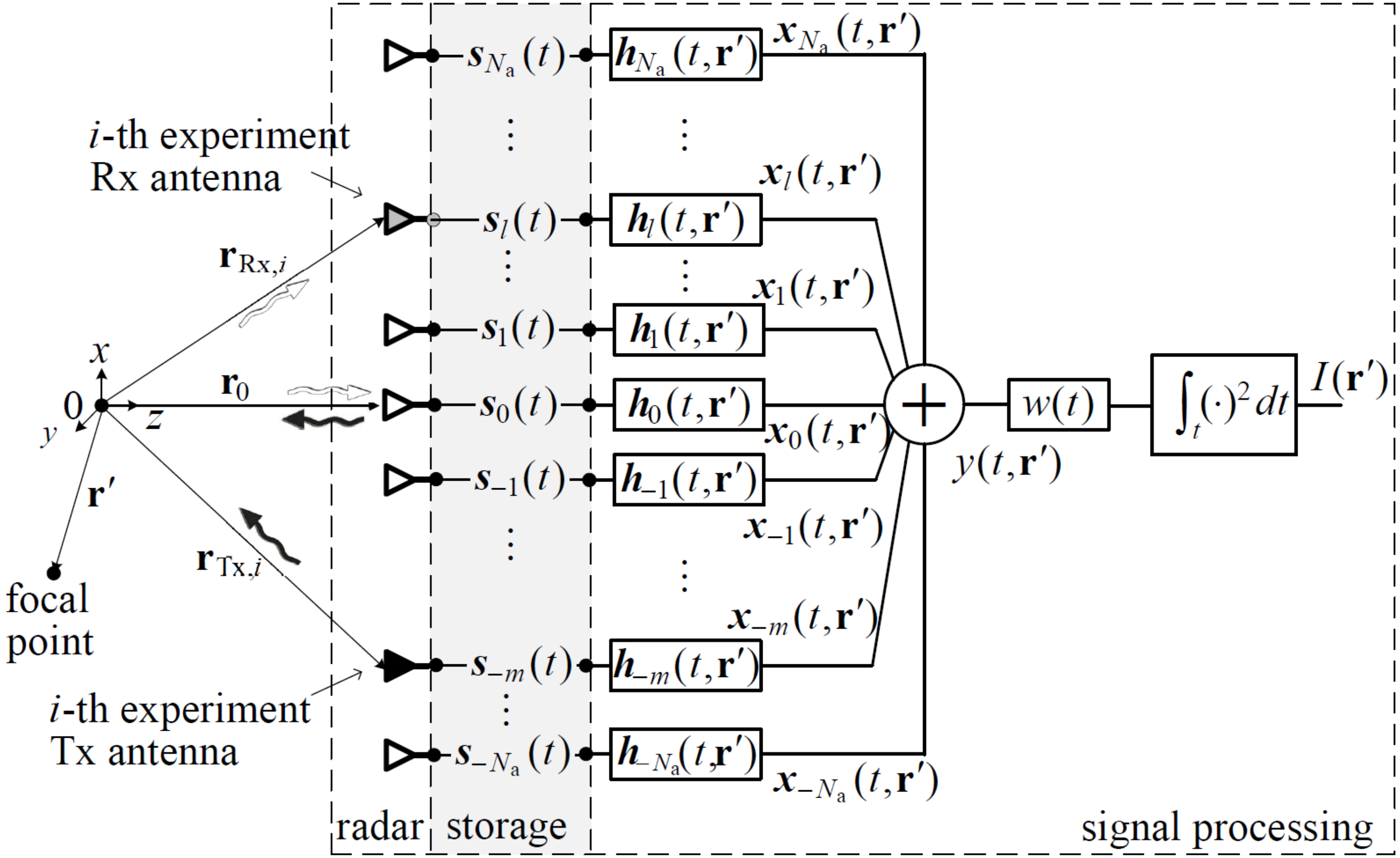

DAS: CONCEPTUAL EXAMPLE

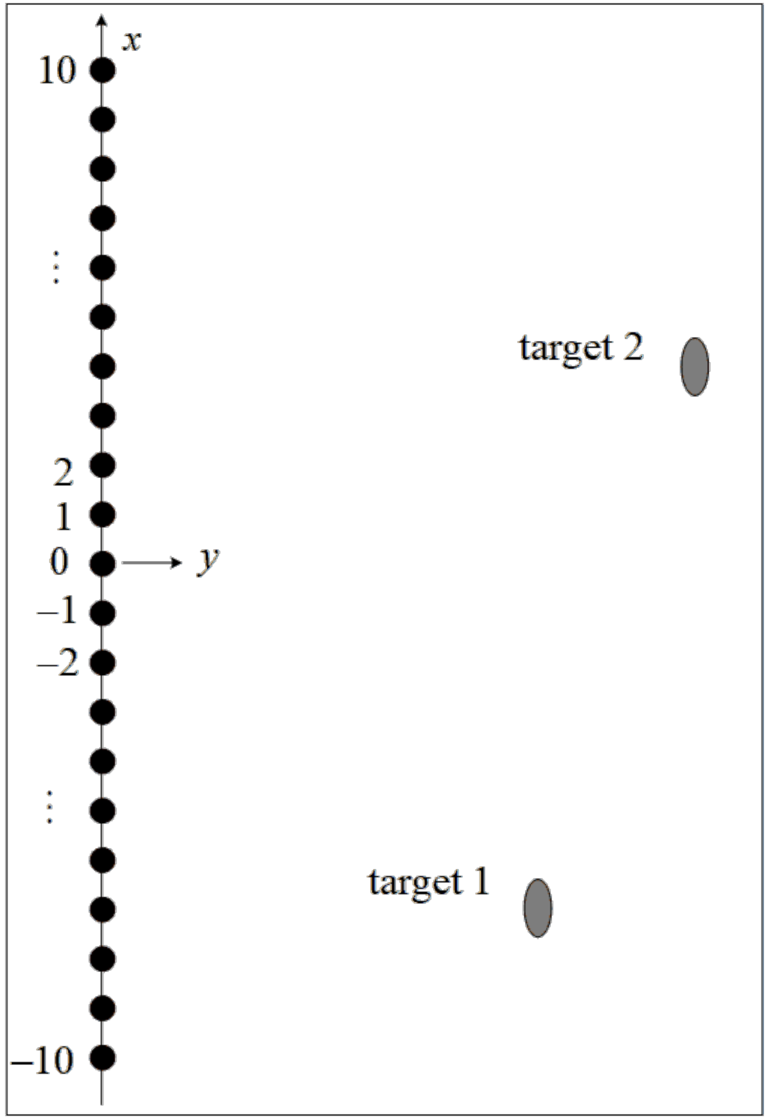

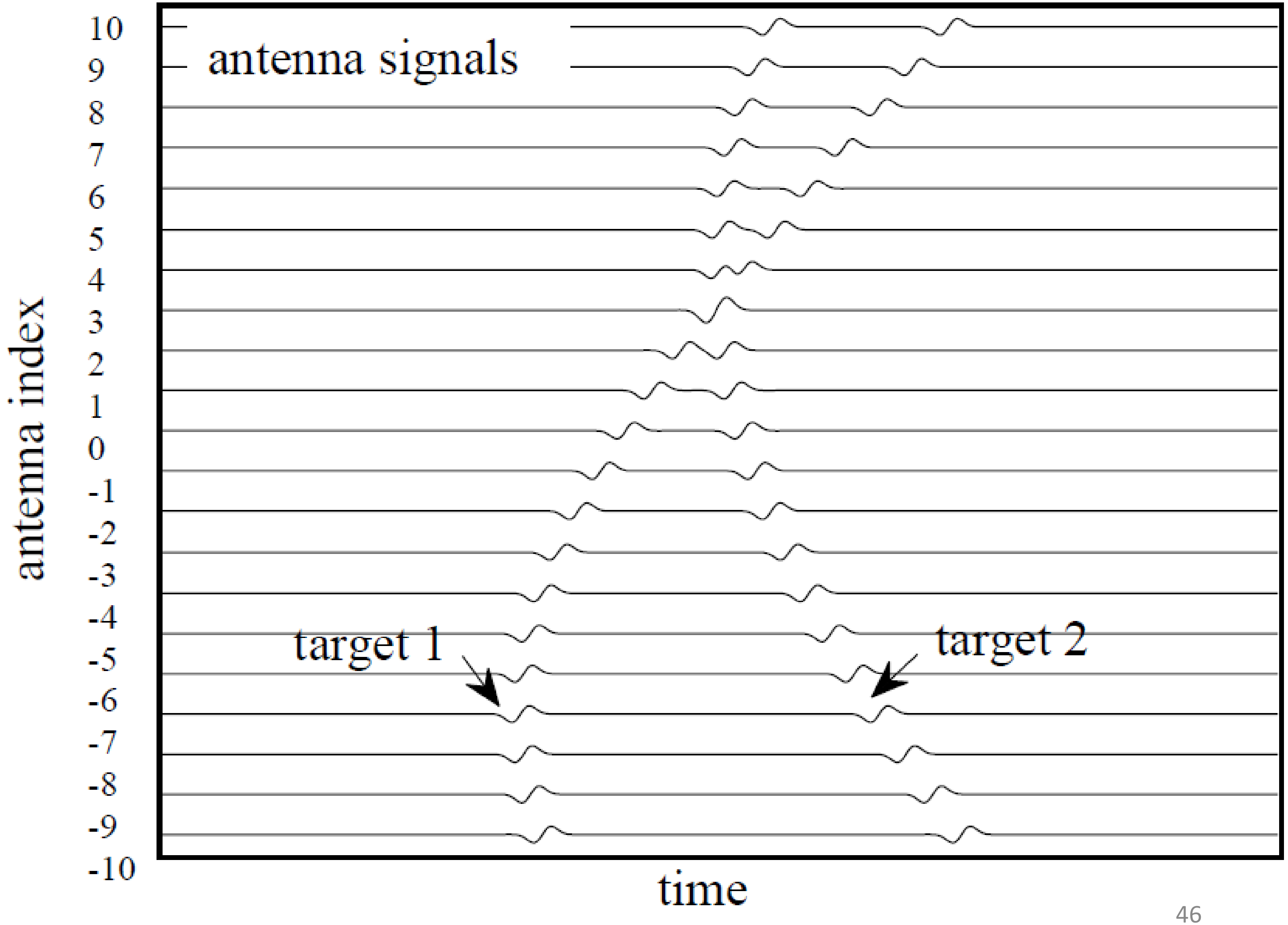

DAS: CONCEPTUAL EXAMPLE – 2

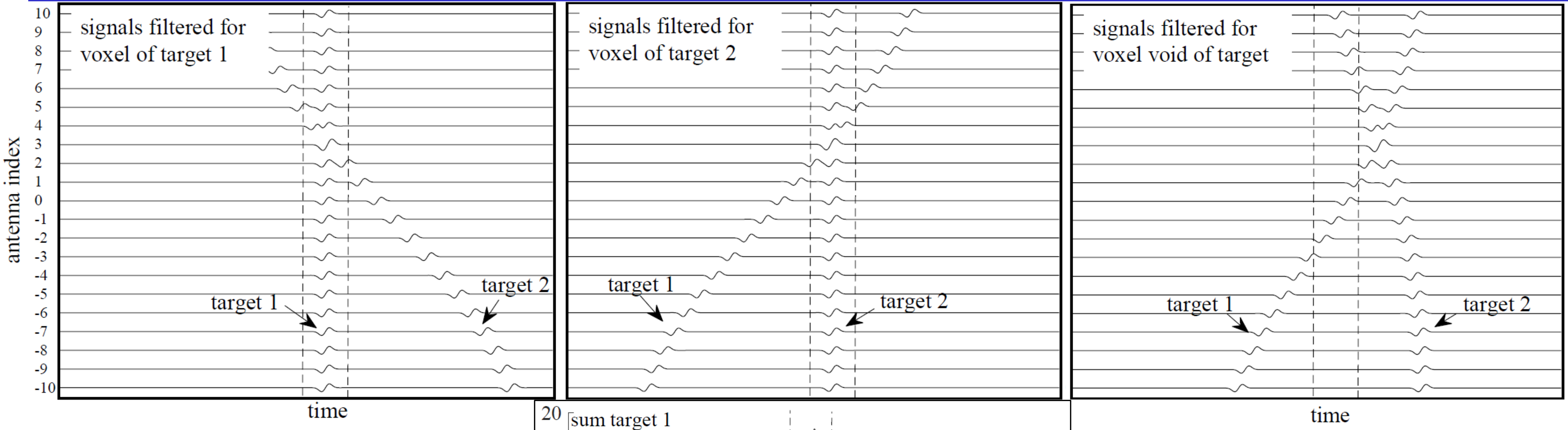

$$X(t,\mathbf{r}')$$

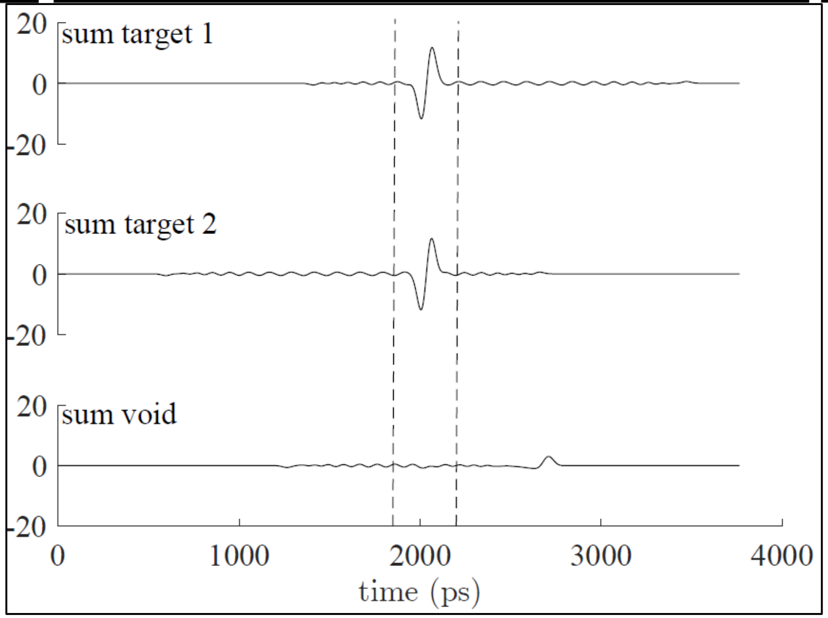

$$I(\mathbf{r}') = \int_t X^2(t,\mathbf{r}')dt$$

$\Downarrow$

plot image

CONCLUDING REMARKS

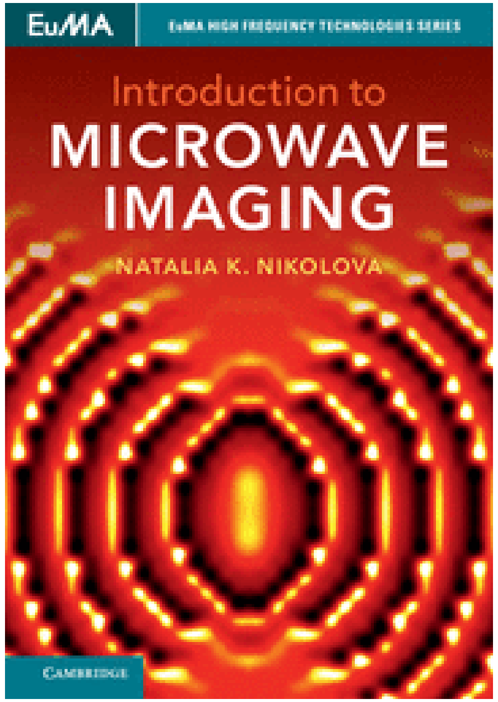

- we have just grazed the surface of an extensive subject
- real-time microwave imaging is rapidly growing and developing
  - ➢ hardware – antennas & RF/radar electronics
  - ➢ calibration methods
  - ➢ inversion methods

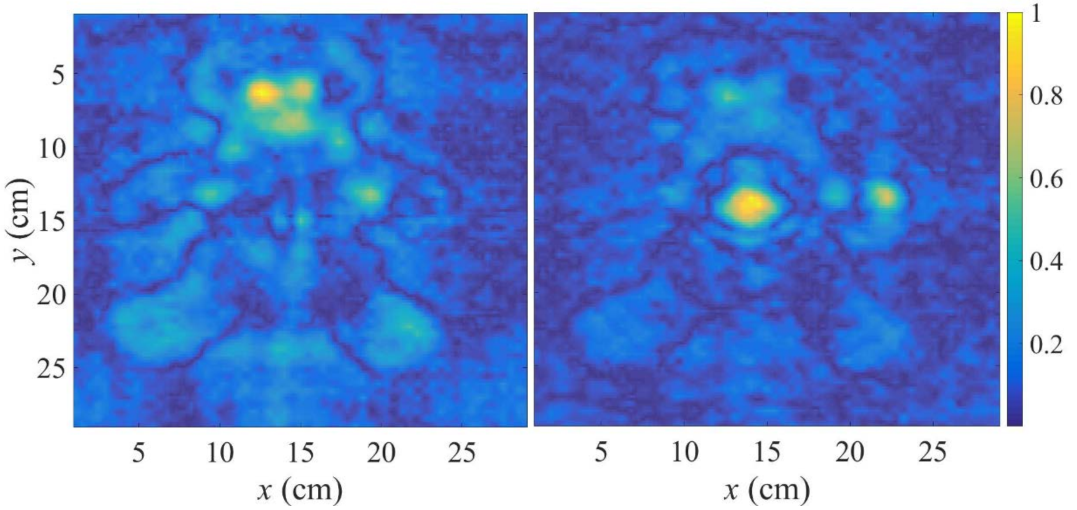

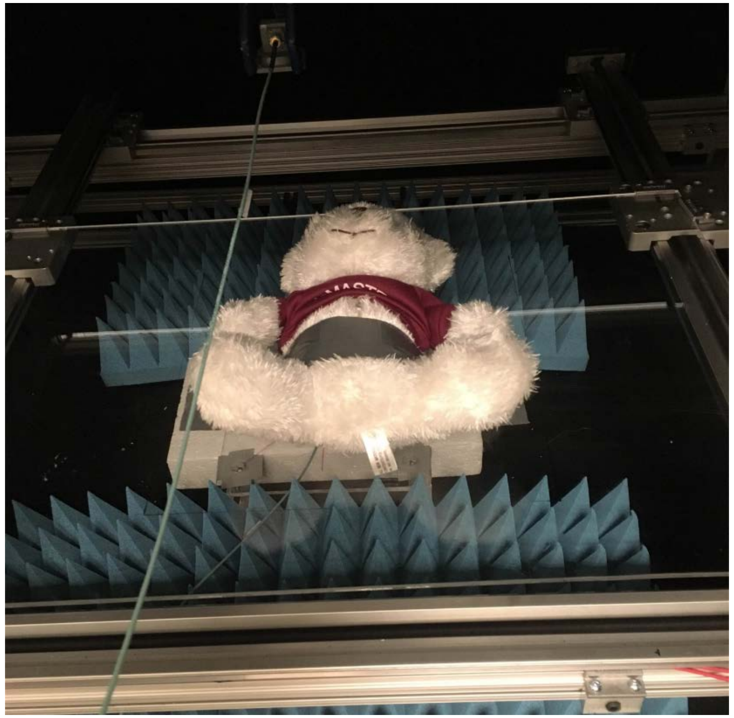

IMAGE SPATIAL RESOLUTION – WHAT TO EXPECT

[Nikolova, *Introduction to Microwave Imaging*, 2017]

- lateral (or cross-range) resolution

$$\delta_{x,y} \ge \frac{\lambda_{\mathrm{eff,min}}}{4} = \frac{\pi}{2k_{x,y}^{\max}}$$

- depth (or range) resolution

$$\delta_z \ge \frac{\lambda_{\mathrm{eff,min}}}{2} = \frac{\pi}{k_z^{\max}} \approx \frac{v_{\mathrm{b}}}{2B}$$

- wide viewing angles are critically important: wide-beam antennas, large scanned apertures

APPLICATIONS: NONDESTRUCTIVE TESTING

[Sheen *et al.*, “Near-field three-dimensional radar imaging techniques and applications,” *Applied Optics* 2010]

Pacific Northwest National Laboratory, Washington, USA

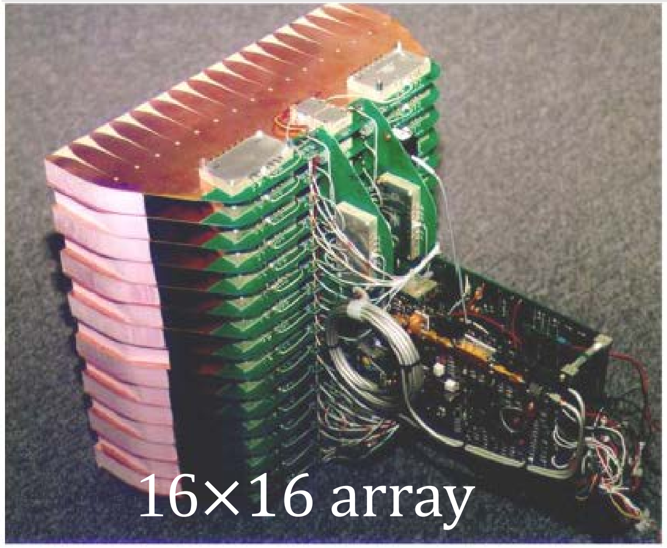

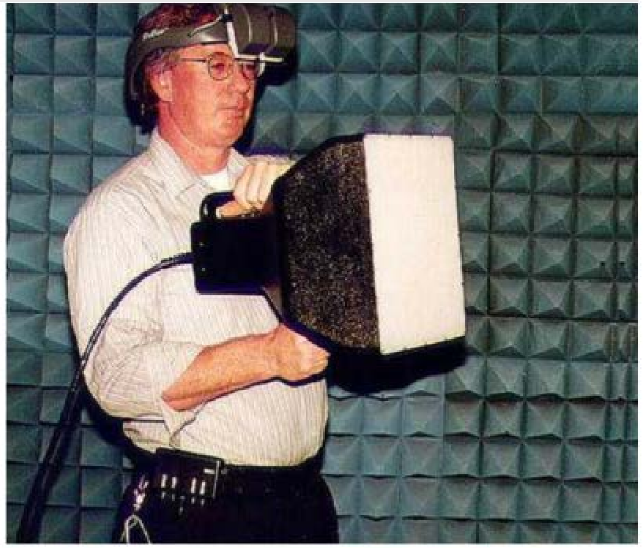

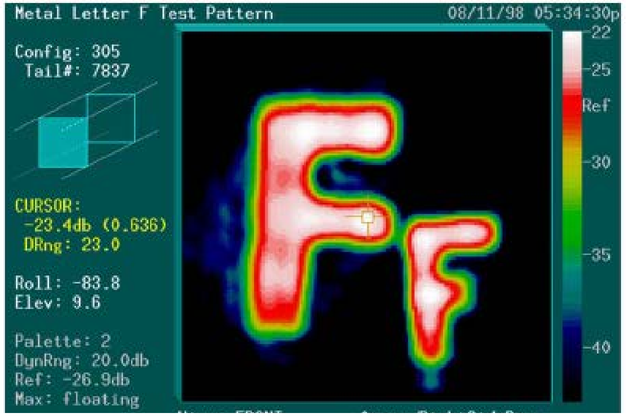

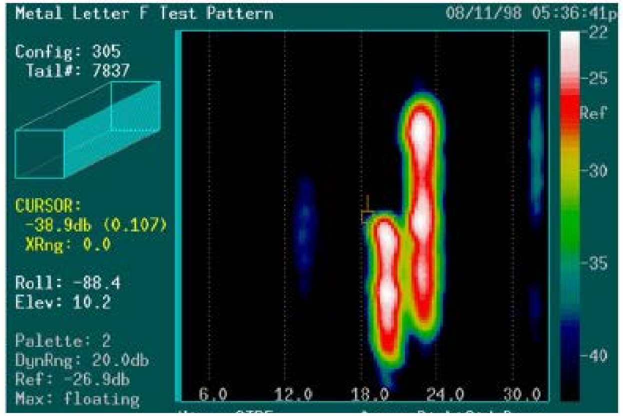

X-BAND (8 TO 12 GHZ) SCANNER WITH 16×16 ELECTRONICALLY SWITCHED ARRAY: ABSORBER INSPECTION

APPLICATIONS: THROUGH-WALL IMAGING

[Depatla *et al.*, “Robotic through-wall imaging,” *IEEE A&P Mag.* 2017]

Prof. Mostofi’s team at the University of California Santa Barbara

Area of interest – top view

3D binary ground-truth image
of the unknown area to be imaged
(2.96 m x 2.96 m x 0.4 m)

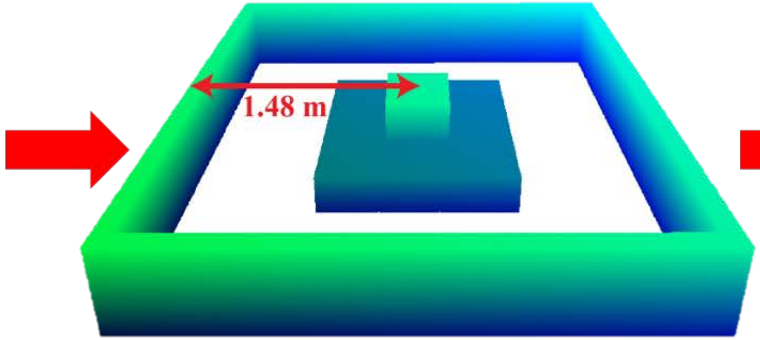

Our 3D image of the area,
based on 3.84 % measurements

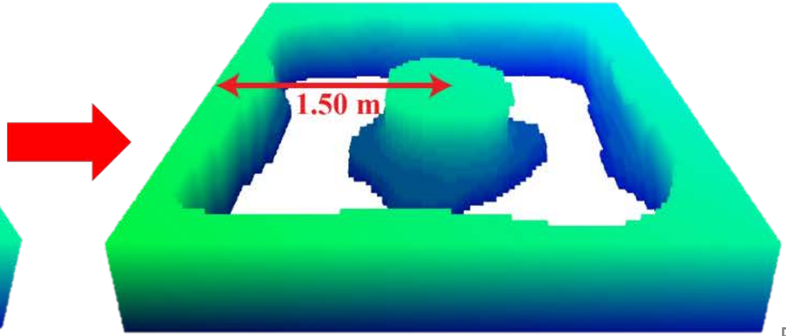

LIMITATIONS OF BORN'S APPROXIMATION: TOTAL INTERNAL FIELD

- limitations on both the size and the contrast of the scatterer

$$\boxed{a^2 \left| k_s^2(\mathbf{r}) - k_b^2 \right| \ll 1, \; \mathbf{r} \in V_s}$$

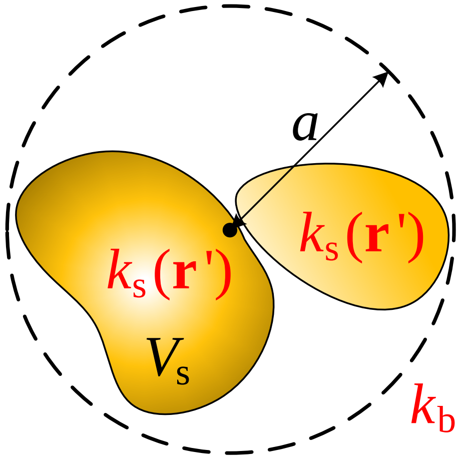

- if OUT violates the limits: images contain artifacts which reflect differences between $\mathbf{E}_{\mathrm{Tx}}^{\mathrm{tot}}(\mathbf{r}')$ and $\mathbf{E}_{\mathrm{Tx}}^{\mathrm{inc}}(\mathbf{r}')$ rather than contrast

EXAMPLE: TOTAL VS. INCIDENT INTERNAL FIELD

60 MM THICK DIELECTRIC SLAB IN AIR

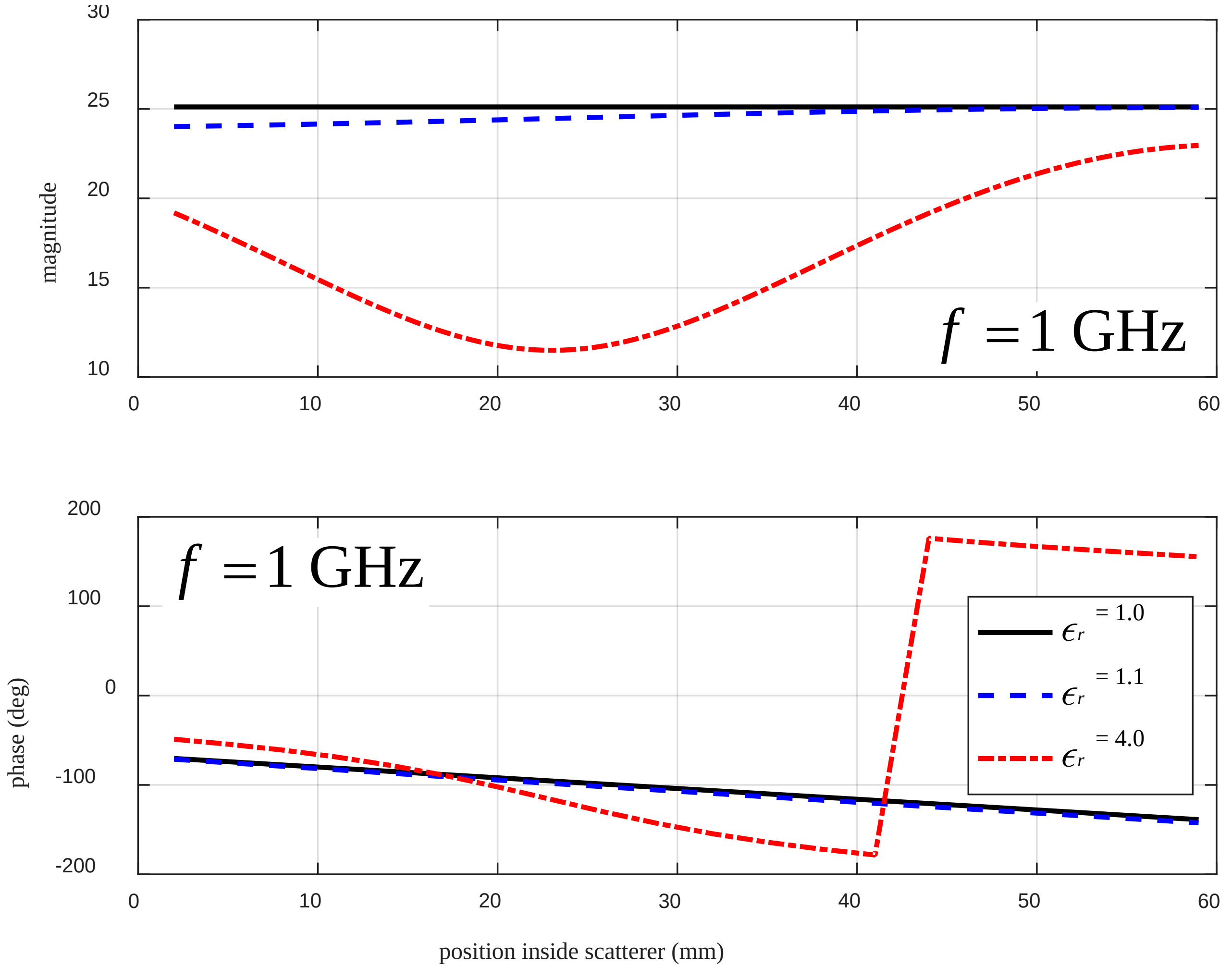

[Nikolova, *Introduction to Microwave Imaging*, 2017]

NUMERICAL ASPECTS OF THE SOLUTION IN FOURIER SPACE

$$\boxed{\tilde{S}_{\xi}^{(m)}(\kappa_{ij}) \approx \sum_{n=1}^{N_z} \tilde{f}(\kappa_{ij}; z'_n)\widetilde{\mathrm{PSF}}_{0z',\xi}^{(m)}(\kappa_{ij})} \qquad \begin{array}{l} m = 1,\ldots,N_\omega \\ \xi = 1,\ldots,N_T \end{array}$$

$$\Rightarrow \boxed{\mathbf{A}(\kappa_{ij})\cdot\mathbf{f}(\kappa_{ij}) = \mathbf{d}(\kappa_{ij})} \qquad \begin{array}{l} \kappa_{ij} = (i\Delta k_x, j\Delta k_y) \\ i = 1,\ldots,N_x;\ j = 1,\ldots,N_y \end{array}$$

solve $(N_x \cdot N_y)$ such systems of size: $N_T N_\omega \times N_z$

the data vector:

$$\mathbf{d}(\kappa_{ij}) = \left[\mathbf{d}_1^T(\kappa_{ij}) \ \cdots \ \mathbf{d}_{N_T}^T(\kappa_{ij})\right]_{N_T N_\omega \times 1}^T, \ \mathbf{d}_{\xi}^T(\kappa_{ij}) = \left[\tilde{S}_{\xi}^{(1)}(\kappa_{ij}) \cdots \tilde{S}_{\xi}^{(N_\omega)}(\kappa_{ij})\right]_{N_\omega \times 1}^T, \ \xi = 1,\ldots,N_T$$

the contrast vector:

$$\mathbf{f}(\kappa_{ij}) = [\tilde{f}(\kappa_{ij}; z'_1) \cdots \ \tilde{f}(\kappa_{ij}; z'_{N_z})]_{N_z \times 1}^T$$

the system (PSF) matrix:

$$\mathbf{A}(\kappa_{ij}) = \begin{bmatrix} \mathbf{A}_1(\kappa_{ij}) \\ \vdots \\ \mathbf{A}_{N_T}(\kappa_{ij}) \end{bmatrix} \text{ where } \mathbf{A}_{\xi}(\kappa_{ij}) = \begin{bmatrix} \widetilde{\mathrm{PSF}}_{0z'_1,\xi}^{(1)}(\kappa_{ij}) & \cdots & \widetilde{\mathrm{PSF}}_{0z'_{N_z},\xi}^{(1)}(\kappa_{ij}) \\ \vdots & \ddots & \vdots \\ \widetilde{\mathrm{PSF}}_{0z'_1,\xi}^{(N_\omega)}(\kappa_{ij}) & \cdots & \widetilde{\mathrm{PSF}}_{0z'_{N_z},\xi}^{(N_\omega)}(\kappa_{ij}) \end{bmatrix}$$

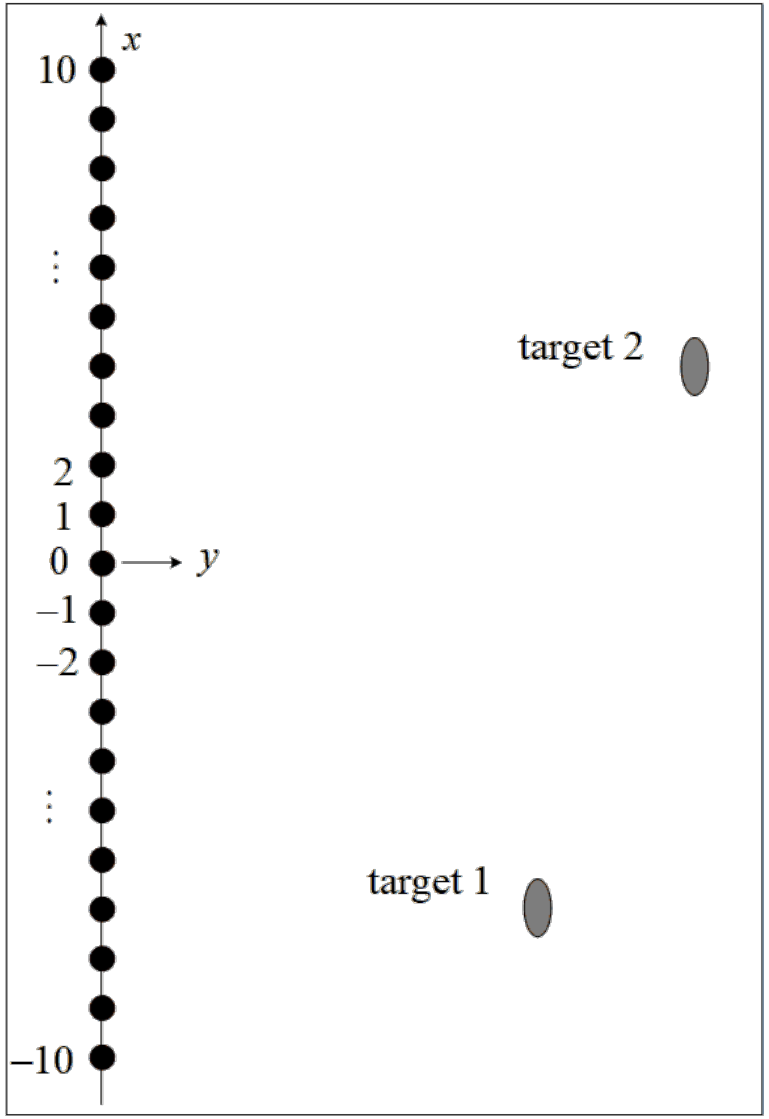
x
10
⋮
2
1
0
y
–1
–2
⋮
–10
target 2
target 1

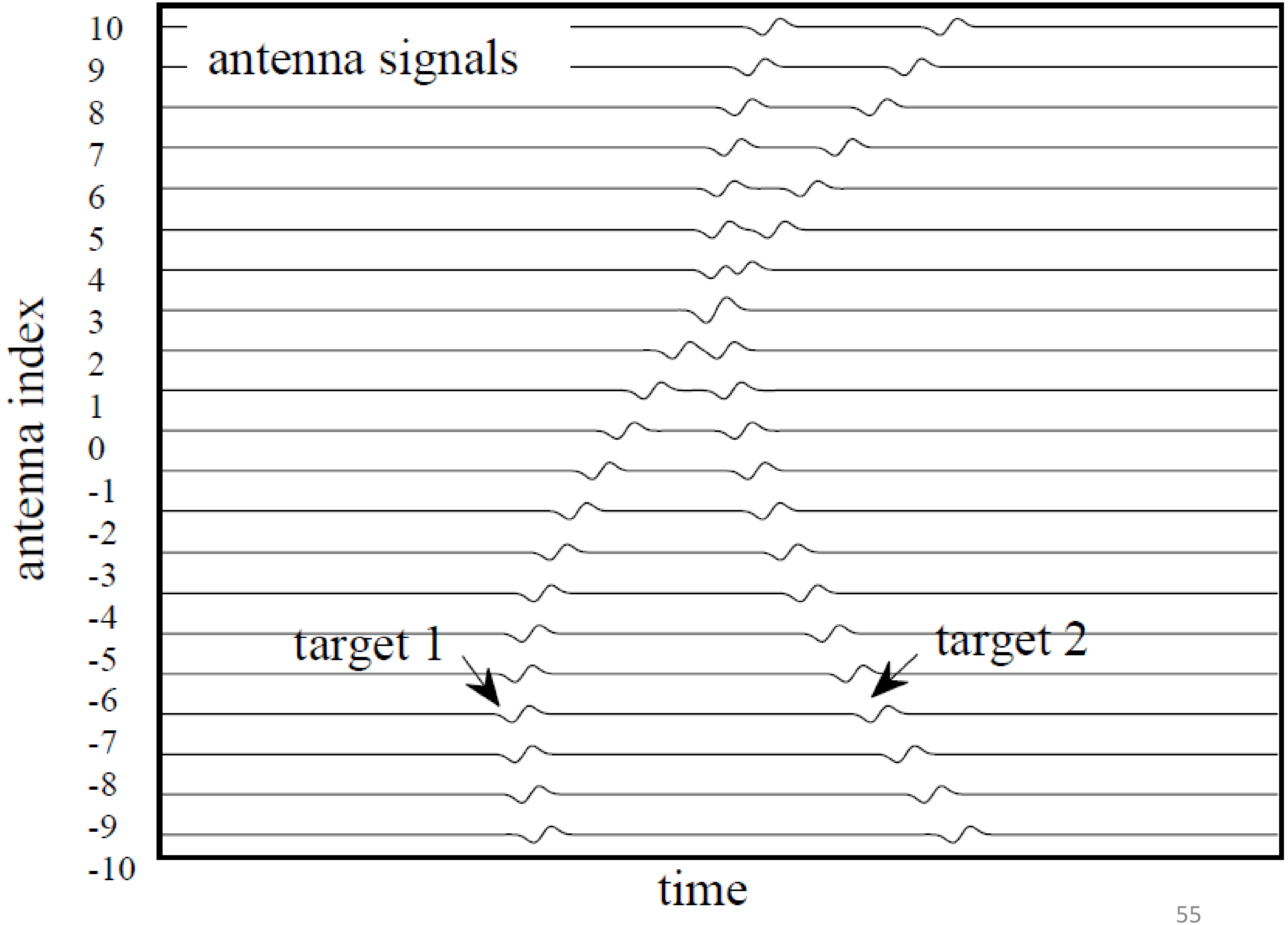
antenna signals
antenna index
10
9
8
7
6
5
4
3
2
1
0
-1
-2
-3
-4
-5
-6
-7
-8
-9
-10
target 1
target 2
time

THE FORWARD MODEL OF HOLOGRAPHY

- the S-parameter forward model

$$\underbrace{S_{\xi}^{\mathrm{sc}}(x, y, \bar{z}; \omega)}_{\text{data}} \approx \iiint_{V_s} \Delta\varepsilon_r(x', y', z') \left[\overline{\mathbf{E}}_{\xi,\mathrm{Rx}}^{\mathrm{inc}} \cdot \overline{\mathbf{E}}_{\xi,\mathrm{Tx}}^{\mathrm{inc}} \right]_{(x',y',z';x,y,\bar{z};\omega)} dx'dy'dz', \quad \xi = 1, \ldots, N_T$$

- ξ (response type) replaces (i,k)

TYPICAL RESPONSE TYPES

ξ	(i,k)	response
1	(1,1)	S_{11}
2	(2,2)	S_{22}
3	(1,2) or (2,1)	$S_{12} = S_{21}$

$N_T = 3$

THE FORWARD MODEL OF HOLOGRAPHY: PLANAR SCAN

- the S-parameter forward model

position of Tx/Rx antenna pair

$$\underbrace{S_\xi^{\mathrm{sc}}(\boxed{x, y, \bar{z}}; \omega)}_{\text{data}} \approx \iiint_{V_s} \Delta\varepsilon_r(x', y', z') \left[\bar{\mathbf{E}}_{\xi,\mathrm{Rx}}^{\mathrm{inc}} \cdot \bar{\mathbf{E}}_{\xi,\mathrm{Tx}}^{\mathrm{inc}} \right]_{(x',y',z';x,y,\bar{z};\omega)} dx'dy'dz', \ \xi = 1, \ldots, N_T$$

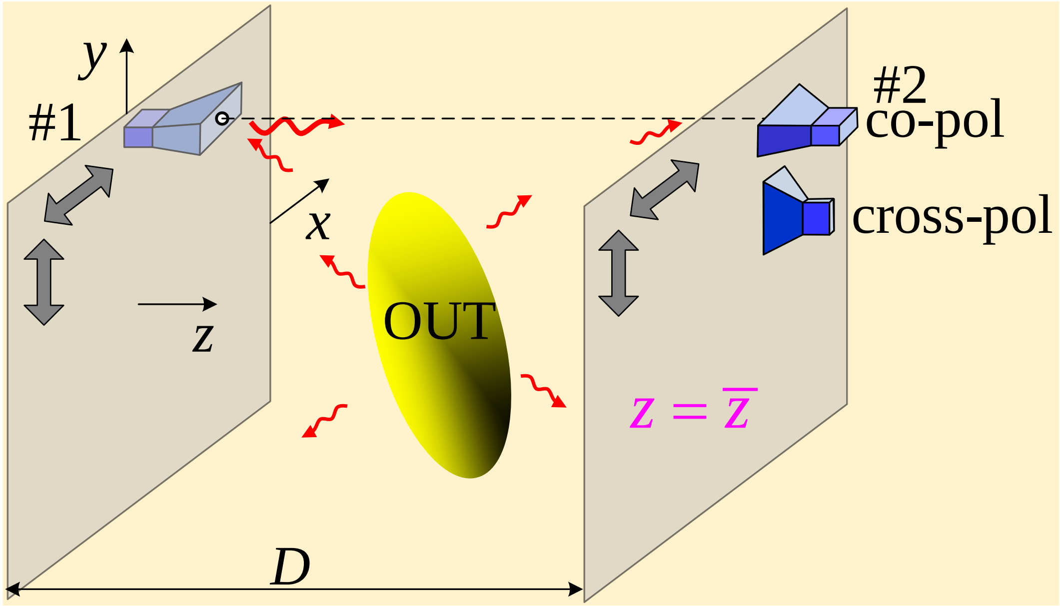

- during scan, the Tx & Rx antennas in each ξ-th experiment are fixed *wrt* each other: if $\mathbf{r}_{\mathrm{Rx}}$ is known then $\mathbf{r}_{\mathrm{Tx}}$ is known, e.g., $\mathbf{r}_{\mathrm{Rx}} \equiv (x, y, \bar{z})$ and $\mathbf{r}_{\mathrm{Tx}} \equiv (x, y, \bar{z} - D)$